Title
The Endogenous Stress Hormone CRH Modulates Excitatory Transmission and Network Physiology in Hippocampus.

Journal
Cerebral cortex (New York, N.Y. : 1991), 27(8)

ISSN
1047-3211

Authors
Gunn, BG
Cox, CD
Chen, Y
et al.

Publication Date
2017-08-01

DOI
10.1093/cercor/bhx103

Cerebral Cortex, August 2017;27: 4182–4198

doi: 10.1093/cercor/bhx103
Advance Access Publication Date: 28 April 2017
Original Article

ORIGINAL ARTICLE

The Endogenous Stress Hormone CRH Modulates Excitatory Transmission and Network Physiology in Hippocampus

B. G. Gunn[1], C. D. Cox[2], Y. Chen[1,2], M. Frotscher[3], C. M. Gall[2,4], T. Z. Baram[1,2,5] and G. Lynch[2,6]

[1]Department of Pediatrics, University of California-Irvine, Irvine, CA, USA, [2]Department of Anatomy/Neurobiology, University of California-Irvine, Irvine, CA, USA, [3]ZMNH, Institute for Structural Neurobiology, D-20251 Hamburg, Germany, [4]Department of Neurobiology and Behavior, University of California-Irvine, Irvine, CA, USA, [5]Department of Neurology, University of California-Irvine, Irvine, CA, USA and [6]Department of Psychiatry and Human Behavior, University of California-Irvine, Irvine, CA, USA

Address correspondence to Prof. T. Z. Baram, Departments of Pediatrics; Anatomy & Neurobiology; Neurology, University of California-Irvine, Medical Sciences I, ZOT: 4475, Irvine, CA 92697-4475, USA. Email: tallie@uci.edu

B. G. Gunn and C. D. Cox contributed equally to the work

Abstract

Memory is strongly influenced by stress but underlying mechanisms are unknown. Here, we used electrophysiology, neuroanatomy, and network simulations to probe the role of the endogenous, stress-related neuropeptide corticotropin-releasing hormone (CRH) in modulating hippocampal function. We focused on neuronal excitability and the incidence of sharp waves (SPWs), a form of intrinsic network activity associated with memory consolidation. Specifically, we blocked endogenous CRH using 2 chemically distinct antagonists of the principal hippocampal CRH receptor, CRHR1. The antagonists caused a modest reduction of spontaneous excitatory transmission onto CA3 pyramidal cells, mediated, in part by effects on I_{AHP}. This was accompanied by a decrease in the incidence but not amplitude of SPWs, indicating that the synaptic actions of CRH are sufficient to alter the output of a complex hippocampal network. A biophysical model of CA3 described how local actions of CRH produce macroscopic consequences including the observed changes in SPWs. Collectively, the results provide a first demonstration of the manner in which subtle synaptic effects of an endogenously released neuropeptide influence hippocampal network level operations and, in the case of CRH, may contribute to the effects of acute stress on memory.

Key words: CRH, hippocampus, sharp waves, stress, neuropeptides

Introduction

Corticotropin-releasing hormone (CRH), a peptide classically associated with activation of the stress response following its release from neuroendocrine cells of the hypothalamus, is expressed in a number of brain regions including the amygdala, bed nucleus of the stria terminalis, and the hippocampus (Sakanaka et al. 1986; Keegan et al. 1994; Yan et al. 1998; Chen et al. 2001). Within the hippocampus, CRH is found in a

population of GABAergic interneurons that innervate pyramidal cells in fields CA1 and CA3 (Chen et al. 2004b, 2012). There are 2 types of CRH receptor, CRHR1 and CRHR2, which are primarily, although not exclusively, expressed at discreet subcellular locations on pyramidal cells within the hippocampus (Chen et al. 2000; Joels and Baram 2009; Refojo et al. 2011). Stress provokes rapid release of hippocampal CRH (Chen et al. 2004b), which may contribute to the established effects of stress on the hippocampus, whereby acute stress enhances and chronic stress impairs memory functions (Kim and Diamond 2002; Joels and Baram 2009; Lupien et al. 2009; Maras and Baram 2012; Chattarji et al. 2015). These effects of CRH on the hippocampus following stressor exposure are mediated by CRHR1 (Chen et al. 2004a, 2010).

Infusions of nanomolar concentrations of CRH into hippocampal slices increase the excitability of CA1 and CA3 pyramidal cells in a dose-dependent manner, an effect that may result from a reduction in the after-hyperpolarization (AHP) that occurs following action potentials (Aldenhoff et al. 1983; Haug and Storm 2000). Exogenous neuropeptide (150 nM) also significantly increases the frequency of spontaneous excitatory postsynaptic currents (sEPSCs) onto CA3 pyramidal cells, with no apparent change in GABAergic transmission (Hollrigel et al. 1998). There are, however, no results addressing the critical question of whether endogenous CRH affects hippocampal functioning under basal conditions. Accordingly, the present studies tested the consequences of application of selective antagonists of CRHR1, upon excitatory and inhibitory inputs to CA3 pyramidal cells. The results from these experiments prompted us to ask if endogenous CRH also influences the operation of complex hippocampal networks. We used sharp waves (SPWs), large composite EPSPs that form part of the SPW-ripple complex, as an endpoint measure. SPWs originate autonomously within subfield CA3b, in part resulting from stochastic release from mossy fibers, and propagate to the remainder of hippocampus via the dense CA3 associational projections (Kubota et al. 2003; Rex et al. 2009). Moreover, the initiation and characteristics of SPWs are regulated by GABAergic interneurons and modulatory inputs to the hippocampus (Kubota et al. 2003; Maier et al. 2003; Rex et al. 2009; Hajos et al. 2013; Schlingloff et al. 2014). SPWs thus provide a quantifiable index for assessing the effects of endogenous CRH on the operation of a large-scale hippocampal network.

The results from these experiments raised the question of whether the observed effects of endogenous CRH are of sufficient magnitude to account for the recorded changes in SPWs, a special case of the general problem of extrapolating network level effects from synaptic physiology. We addressed the issue using a detailed model of the complex circuitry generated by hippocampal field CA3.

Together, the findings reported here constitute the first functional evidence for a role played by an endogenous neuropeptide, CRH, across multiple levels of hippocampal physiology and functioning.

Methods

Animals

In accord with recent NIH guidelines for rigor and reproducibility, we have aimed to conduct experiments that will yield robust, unbiased results. All procedures were performed in accordance with the National Institute of Health Guide for Care and Use of Laboratory Animals and were approved by the Institutional Care and Use Committee of the University of California, Irvine. Male mice were group housed on a 12:12 light:dark cycle and provided with access to water and standard rodent chow ad libitum. Whole cell and extracellular recordings were made from animals derived from at least 3 different litters. A total of 45 animals were used for whole-cell patch-clamp recordings, while extracellular recordings were made from 9 animals.

Electrophysiology

Whole-Cell Recordings

Ventral hippocampal brain slices were prepared from male C57BL6 mice (PND 21–40). Briefly, brains were rapidly removed and placed in ice cold, oxygenated (95% O_2) artificial cerebrospinal fluid (aCSF) containing (in mM): 87 NaCl, 75 sucrose, 26 $NaHCO_3$, 2.5 KCl, 1.25 NaH_2PO_4, 0.5 $CaCl_2$, 7 $MgCl_2$, and 10 glucose (320–335 mOsm). Horizontal brain slices (350–400 μM) were then cut using a vibratome (Leica VT 1000) at 0–4 °C. Slices were subsequently incubated in a recovery chamber at room temperature for up to 1 h in oxygenated aCSF (as above), before being transferred to a holding chamber and incubated at room temperature in oxygenated extracellular solution (ECS) containing (in mM): 124 NaCl, 3 KCl, 1.25 NaH_2PO_4, 2.5 $CaCl_2$, 1.25 $MgSO_4$, 26 $NaHCO_3$, and 10 glucose (300–310 mOsm, pH ~ 7.4). Slices were then transferred to the recording chamber as required.

Whole-Cell Voltage-Clamp Recordings

Whole-cell voltage-clamp recordings of miniature and spontaneous excitatory and inhibitory postsynaptic currents (mEPSC/sEPSC and sIPSC, respectively) were made from CA3 pyramidal cells at 26–28 °C in ECS (as above) in the presence and absence of 0.5 μM TTX (Tocris Biosciences), respectively. Patch pipettes (R = 5–8 MΩ) were filled with a low Cl^- intracellular solution containing (in mM): 135 CH_3O_3SCs, 8 CsCl, 10 HEPES, 10 EGTA, 1 $MgCl_2$, 1 $CaCl_2$, 2 Mg-ATP and 0.3 Na-GTP, 300–310 mOsm, pH 7.2–7.3 with CsOH. Under such recording conditions, the calculated (pClamp version 10.2) and experimentally verified E_{GABA} and $E_{Glutamate}$ was −63 and 0 mV, respectively. This allows mEPSC/ sEPSC and sIPSC to be recorded without $GABA_AR$ or ionotropic glutamate receptor antagonists present, respectively (i.e., local network integrity maintained). After >10 min stable control recording, the CRHR1 antagonist (NBI 30775 [1 μM] generous gift of Dr D. Grigioradis or α-helical$CRH_{(9-41)}$ [1 μM], Bachem) was bath applied to the slice for at least 15 min. In a subset of experiments, the respective CRHR antagonist was washed for 30–60 min. The $GABA_AR$-mediated tonic current was quantified (using the same conditions as above for IPSCs) following treatment with bicuculline (20 μM, Abcam) and the effect that inhibition of CRH had upon this current was assessed.

Whole-cell voltage-clamp recordings of Ca^{2+}-dependent K^+-currents that mediate the AHP (I_{AHP}) were recorded from CA3 pyramidal cells at 30–32 °C in ECS (as above) that additionally contained 0.5 μM TTX and 20 μM SR95531. Patch pipettes (R = 5–8 MΩ) were filled with an intracellular solution containing the following (in mM): 135 K-gluconate, 10 HEPES, 4 KCl, 1 $MgCl_2$, 2 Mg-ATP, 0.3 Na-GTP and 10 Tris-phosphocreatine, 300–310 mOsm, pH 7.2–7.3 with KOH. CA3 pyramidal cells were clamped at a holding potential of −50 mV and I_{AHP}'s were elicited once every 60 s by a 50–100 ms long depolarizing step to 0 mV before and after the bath application of the CRHR1 antagonist NBI 30775 (1 μM). A liquid junction potential of 14 mV was corrected for in the recordings as previously described (Neher 1992).

Currents were filtered at 5 kHz using an 8-pole low-pass Bessel filter. The series resistance was between 10 and 25 MΩ with up to 70% compensation. Only cells that had a stable access resistance

were used and recordings were aborted if >20% changes in series resistance occurred. All recordings were performed using an Axopatch 1D amplifier (Molecular Devices) and pClamp 9. Recordings were stored directly to a PC (10 kHz digitization) using a Digidata 1322A (Molecular Devices) for analysis offline.

Whole-Cell Current-Clamp Recordings

Spontaneous action potentials from CA3 pyramidal cells were made at 30–32 °C in ECS (as above), using patch pipettes (R = 5–8 MΩ) filled with an intracellular solution containing the following (in mM): 135 K-gluconate, 10 HEPES, 4 KCl, 1 $MgCl_2$, 2 Mg-ATP, 0.3 Na-GTP and 10 Tris-phosphocreatine, 300–310 mOsm, pH 7.2–7.3 with KOH. Cells were maintained at a membrane potential ($V_{membrane}$) where action potential firing occurred in probabilistic, rather than deterministic manner (Prescott et al. 2006). Action potential properties were assessed before and after the bath application of NBI 30775 (1 μM). A liquid junction potential of 14 mV was corrected for in the recordings as previously described (Neher 1992). Currents were filtered at 5 kHz using an 8-pole low-pass Bessel filter. All recordings were performed using an Axopatch 1D amplifier (Molecular Devices) and pClamp 9. Recordings were stored directly to a PC (10 kHz digitization) using a Digidata 1322A (Molecular Devices) for analysis offline.

Extracellular Recordings

Ventral hippocampal slices were prepared as previously described (Kubota et al. 2003) from male C57BL6 mice (8–12 wks). Brains were rapidly removed and placed in ice cold, oxygenated (95% O_2) aCSF containing (in mM): 124 NaCl, 26 $NaHCO_3$, 3 KCl, 1.25 NaH_2PO_4, 3.75 $MgSO_4$, and 10 glucose (pH 7.4, 315–320 mOsm). Horizontal slices (400 μM) were cut using a Leica VT1000 at 0–4 °C and placed on an interface recording chamber. Oxygenated aCSF containing (in mM): 124 NaCl, 26 $NaHCO_3$, 3 KCl, 1.25 KH_2PO_4, 3 $CaCl_2$, 1 $MgSO_4$, and 10 glucose (pH 7.4, 300–310 mOsm) were perfused at a rate of 60 mL/h. Slices were allowed to recover for >1 h prior to recording, while warmed and humidified 95% O_2–5% CO_2 filled the chamber throughout the experiment.

Glass pipettes containing 2 M NaCl were used to record SPWs from the apical dendrites of CA3 pyramidal cells at 30–32 °C. As the occurrence of SPWs was variable between slices, we sampled each slice and selected the one that had the most stable frequency of SPWs to carry out our experiments. Baseline measures were established for 50–60 min prior to the introduction of NBI 30775 (1 μM) via a second infusion line. Recordings were digitized at 20 kHz using an AC amplifier (A-M Systems, Model 1700) and sweeps of 10 s duration were recorded every 10 s (i.e., continuous) using NAC 2.0 Neurodata Acquisition System (Theta Burst Corp.).

Data Analysis

Voltage-Clamp Recordings: Analysis of Synaptic Currents

All recordings were analyzed offline using the Strathclyde Electrophysiological Software (WinEDR and WinWCP, Dr J. Dempster, University of Strathclyde).

Excitatory and inhibitory events were detected in WinEDR using an amplitude threshold detection algorithm (EPSCs: −4 pA, 1–3 ms duration; IPSCs: 4 pA, 1–3 ms duration) and visually inspected for validity before being exported to WinWCP. In general, >40 accepted events were used to generate an averaged EPSC/IPSC, however, in some cells with a particularly low frequency, averaged currents were generated from as few as 12 events. Events were analyzed with regard to peak amplitude, rise time (10–90%) and decay kinetics. The decay phase of the digitally averaged EPSC and IPSC was best described by a single exponential equation [$Y(t) = A^*\exp(-t/\tau)$]. The frequency of events was measured in separate 1 min bins (at least 3 bins) over a period of at least 8 min, before and after (at least 10 min) treatment with the CRH antagonist. Events were detected using an amplitude threshold (as above) and visually inspected for validity and to ensure no events were missed.

Voltage-Clamp Recordings: Analysis of Tonic Current

The GABAergic tonic current and drug-induced current was calculated as the difference between the mean baseline current before and after bath application of bicuculline or CRHR1 antagonist. The holding current and root mean square (RMS) were sampled every 25.6 ms over a 1 min period for each recording condition (i.e., presence and absence of drug). At a sampling rate of 10 kHz, 256 baseline points for each 25.6 ms provided one data point. Epochs containing IPSCs or unstable baseline were excluded from the analysis and a minimum of 100 data points were measured for each recording condition. In order to determine whether a drug effect was genuine and not simply due to temporal "drift" in the holding current, 2 separate 60 s sections were analyzed during the control period (C1 and C2; typically the first and last 60 s of the control period). Similarly, a 1 min section was analyzed after drug application (D) once the drug effect had reached a plateau. Similar temporal intervals were selected between C1, C2, and D to control for temporal drift during the control period and after drug application. The mean DC values for C1 and C2 were pooled and the SD calculated. A drug effect was considered genuine if the absolute change in holding current (i.e., D-C2) was greater than twice the SD associated with the DC measurements of the control period (i.e., C1 and C2 pooled).

Voltage-Clamp Recordings: Analysis of I_{AHP}

The I_{AHP} currents were manually detected offline using WinEDR and then exported to WinWCP where they were analyzed with regard to peak amplitude, rise time and decay time course. At least 3 accepted events were used to generate an averaged I_{AHP} in the absence and presence of NBI 30775 for each cell. The decay phase of the digitally averaged I_{AHP} was best described by the bi-exponential equation ($Y(t) = A_1^*\exp(-t/\tau_1) + A_2^*\exp(-t/\tau_2)$). A weighed decay constant (τ_W) was then calculated to describe the relative contribution of each decay component using the following equation: $\tau W = [A_1/(A_1 + A_2)]^*\tau_1 + [A_2/(A_1 + A_2)]^*\tau_2$, where A_1 and A_2 describe the relative contribution that τ_1 and τ_2 make, respectively.

Current-Clamp Recordings: Analysis of Action Potentials

Action potentials were detected in Clampfit 10.2 using an amplitude threshold detection algorithm (Δ of 50–55 mV in $V_{membrane}$) and visually inspected for validity. In general, at least 15 accepted events were used to assess action potential properties and to generate an averaged event in the absence and presence of the antagonist. Action potentials were analyzed with regard to peak amplitude (total spike), rise time (10–90%), half-width, decay time (90–10%), and the amplitude and decay time of the AHP in the absence and presence of NBI 30775 (1 μM). The action potential frequency was analyzed using WinEDR. Events were detected using a rate of rise

algorithm (~20 mV/ms) and visually inspected for validity. The frequency was measured over a 1 min period before and >10 min after bath application of the CRHR1 antagonist. The $V_{Membrane}$ of the cell was estimated before and after bath application of NBI 30775 (1 μM). The membrane potential was sampled every 204.8 ms over a 1 min section for each recording condition (i.e., absence and presence of drug). At a sampling rate of 10 kHz, each data point was comprised of 2048 baseline points for each 204.8 ms. Epochs containing action potentials or extreme swings in $V_{Membrane}$ were excluded from the analysis.

Analysis of SPWs

SPWs were analyzed off line using a custom-written computer code using Python, version 2.7.8, NumPy, and Scipy. SPWs were analyzed off line using a custom-written computer code. To calculate the frequency of SPWs, each 10 s epoch of signal, was fed through a second order Butterworth filter in the range 2–45 Hz. This removed any baseline drift and smoothed out the high-frequency events while preserving the amplitude of SPW events. Samples with massive down swings were dropped if more than 7.5% of their signal was below −0.06 mV in the filtered signal. Event seeds were started if the trace passed −0.025 mV. After such an event, the nearest point crossing 0 mV before and after the event was found. The lowest point was recorded as the amplitude and the mean SPW amplitude was reported for each 10 s time bin. The frequency was the count of events per second averaged over each 10 s time bin. The within slice frequency range was described by the instantaneous frequency which was calculated from the interevent intervals (IEI). The peak amplitude, area, and rise time (10–90%) were calculated from the filtered (2–45 Hz) signal. The decay time (τ) was calculated from the unfiltered signal using a mono-exponential decay [$Y(t) = A^*\exp(-t/\tau)$] and events with a decay τ of <10 ms or >250 ms were discarded from the analysis.

Simulations: Hippocampal Neuronal Network

General Properties and Architecture of Model

We modified a previously reported CA3-CA1 hippocampal model that produces simulated SPWs (Taxidis et al. 2012) to include a dentate gyrus (DG) component, and used this model to assess the influence that synaptic transmission at the single cell level has upon the generation of these network events. Briefly, the DG was comprised of 1000 cells with no recurrent connections and a low probability (1 in 1000) of connectivity to CA3 pyramidal cells. The DG activity was determined using a Poisson distribution around a set frequency. The CA3 and CA1 were comprised of 1000 pyramidal cells and 100 interneurons each (i.e., 10:1 pyramidal cell to interneuron ratio). The distance between neurons was 10 μM for both regions, with interneurons positioned equidistantly (1 every 10 cells) throughout the array. Pyramidal cells were modeled by the 2-compartment Pinsky–Rinzel model (Pinsky and Rinzel 1994) adapted from ModelDB (accession no 35358; Migliore et al. 2003) while interneurons were modeled on the single-compartment Wang–Buzsaki model (Wang and Buzsaki 1996). In CA3, pyramidal cells were recurrently connected to each other as well as to inhibitory interneurons, providing strong feedforward and feedback inhibition. In contrast, CA1 interneurons were strongly connected with one another without recurrent excitatory connections. The CA3 and CA1 arrays were separated by a distance of 100 μM, with CA3 pyramidal cells connecting to both pyramidal cells and interneurons within the CA1. A Gaussian distribution was used to determine the probability of connectivity among cell types as previously described (Taxidis et al. 2012, Supplementary Fig. 1 and Table 1). In both the CA3 and CA1, excitatory and inhibitory synaptic interactions among cells were mediated by AMPA and $GABA_A$ receptors, respectively. Synaptic interactions were modeled as previously described where the synaptic conductance was set to 1 nS for all synapses (Taxidis et al. 2012; see Supplemental Methods). As such, the strength of synaptic events was controlled by the variable α_{syn}. Values for α_{syn} were specific for each excitatory and inhibitory synapse among cells (Supplementary Table 1). The decay time (τ) of excitatory currents was set to 2 ms, and for $GABA_A$R-mediated currents at 7 and 2 ms for synapses targeting pyramidal cells and interneurons, respectively. Conductance velocity for pyramidal cell axons (CA3 and CA1) was 0.5 mm/ms, and for CA1 and CA3 interneurons conductance velocities were set as 0.1 mm/ms and instantaneous, respectively (Taxidis et al. 2012). Heterogeneity in the system was introduced through variation in the reversal potential of neurons that was distributed over cells using a Gaussian distribution. A firing reset voltage of −60 mV was introduced. To prevent oscillations in cell voltages (and model collapse) the maximum number of synaptic inputs to an individual cell, at the same time, was capped at 100.

Modulating Frequency of EPSCs onto CA3 Pyramidal Cells

We used the DG-CA3-CA1 model to examine the effect that changes in the frequency of EPSCs onto CA3 pyramidal cells on the generation of SPWs in both the CA3 and CA1 arrays. The frequency of simulated EPSCs onto CA3 pyramidal was sensitive to (1) the frequency of DG activity and (2) the strength of excitatory synaptic conductance (scaled DG and CA3 synapses). Frequency of DG activity was increased at 0.5 Hz increments (range 0.5–4 Hz) and the frequency of EPSCs in CA3 pyramidal cells and the number of SPWs in CA3 and CA1 were quantified. The synaptic strength onto CA3 pyramidal cells was similarly increased in 0.5 increments (arbitrary units [a.u.]. Range 0.5–3.5) and frequencies of EPSCs and SPWs similarly assessed. The hippocampal model was run over a 10 s period and repeated 10 times for each DG frequency and synaptic strength value.

Modulating the Residual Depolarizing Current onto CA3 Pyramidal Cells

The effect that the residual depolarizing current onto CA3 pyramidal cells had upon generation of SPWs in CA3 and CA1 was assessed using the adapted CA3-CA1 model (i.e., without a DG component). A depolarizing current was applied to CA3 pyramidal cells for the duration of each simulation (i.e., 10 s), with a range in amplitude of 0.15–0.24 nA, and the frequency of SPWs in the CA3 and CA1 arrays were measured. The model was run over a 10 s period and repeated 10 times for each different current step.

Assessing the Effect of DG Cell Synchronization upon the Probability of SPW Generation in CA3

The effect that synchronization of multiple mossy fiber inputs had upon SPW generation in the CA3 array was assessed by determining how the number of DG cell firing (% of total) over different periods of time (10, 50, 100, and 200 ms) influenced the probability of a single SPW occurring. We identified a threshold that seemed to be of physiological relevance, in this case 200 DG cells (i.e., 20% of total) and the probability of a SPW

being generated was calculated from a 1 s period that was repeated 30 times for each time period (i.e., 10, 50, 100, and 200 ms). We used a synaptic strength measure of 1.5 a.u. for our baseline measure that was reduced to 1.4 a.u. to model potential effects of CRHR1 inhibition.

Detection and Analysis of Hippocampal Simulations

A SPW was defined as >100 cells firing within a 50 ms time period in the CA3 array and >500 cells firing within the same time epoch in CA1. Adjacent epochs that were also above threshold were considered the same event. The frequency of SPWs was calculated as the number of events over the 10 s run time. SPW traces were generated from 55 firing cells, consisting of both pyramidal cells and interneurons, and were displayed as the average $V_{membrane}$ across these cells. The potential difference (i.e., $V_{membrane}$) was recorded from the dendritic and somatic compartment of pyramidal cells and interneurons, respectively. A similar approach was used to generate the firing properties of individual CA1 pyramidal cell and interneuron firing patterns during a SPW.

The frequency of EPSCs was determined using an amplitude threshold (−5 mV) with a baseline reset of −2 mV. The hippocampal model was run over a 10 s period and repeated 10 times for each DG frequency and synaptic strength. SPW frequency was calculated from the number of events per 10 s simulation run.

All code (SPW and modeling) was written using BRIAN simulator v2 (Stimberg et al. 2014). The model in its entirety is available at: http://modeldb.yale.edu/225906.

Electron Microscopy

Detection of CRH receptor CRHR1 was accomplished as described previously (Chen et al. 2004b). Briefly, horizontal slices (300 μM) were made using a vibratome, the CA3 region of the hippocampus excised and post-embedding immunogold labeling performed. The tissue blocks were cryoprotected in glycerol, cryofixed in nitrogen-cooled propane, substituted in methanol containing 1.5% uranyl acetate and embedded in Lowicryl HM20. Ultrathin sections were processed for post-embedding immunostaining, employing the CRHR1 antiserum (1:100). Immunolabeling was visualized using 6 nm gold-coupled secondary antibodies (rabbit anti-goat; 1:20, Aurion).

Statistical Analysis

All data are presented as the mean ± SEM unless otherwise stated. Statistical comparisons were made using Student's *t*-test (paired and unpaired, 2-tailed) and repeated measures ANOVA (1- and 2-way), followed by the post hoc Bonferroni as appropriate. When normalized data are presented, mean values have been calculated by averaging the normalized changes for each cell, along with the associated SEM. Statistics were performed using GraphPad Prism 5.

Results

Inhibition of CRHR1 Reduces the Frequency of Excitatory Synaptic Currents in CA3 Pyramidal Cells

We initially characterized the properties of sEPSCs recorded from CA3 pyramidal cells at the holding potential for E_{GABA} (−63 mV). $GABA_AR$ antagonists were not used so that regulation of input from other pyramidal cells by inhibitory interneurons was unperturbed (Table 1). The bath application of the nonselective ionotropic glutamate receptor antagonist, kynurenic acid (2 mM) abolished synaptic currents confirming that the recorded events were exclusively glutamatergic ($n = 3$, not shown). Inhibition of CRHR1 following the bath application of the selective small molecule allosteric antagonist, NBI 30775 (1 μM), significantly reduced the frequency of sEPSCs (71 ± 6% CTRL frequency, $n = 8$, $P < 0.05$ 1-way RMA, Fig. 1A,C, Table 2A). Blocking CRHR1 had no effect upon peak amplitude or rise time ($P > 0.05$ paired Student's *t*-test) of sEPSCs, while the decay time course (τ) was prolonged ($P < 0.05$ paired Student's *t*-test. Fig. 2A, Table 2A). Consistent with the slow dissociation constant of NBI 30775 from CRHR1 (Chen and Grigoriadis 2005), the effects of the antagonist upon sEPSC frequency were slow to reverse during a 20–60 min washout (78 ± 9% of CTRL, $n = 4$. Fig. 1D). To exclude nonspecific actions of NBI 30775 on sEPSC properties, and to enable washout, we employed a second, nonspecific competitive antagonist, α-helical $CRH_{(9-41)}$, a peptide that binds to a different site on the CRHR1. Bath application of α-helical $CRH_{(9-41)}$ (1 μM) resulted in a similar reduction in the frequency of sEPSCs (62 ± 5% CTRL frequency, $n = 5$, $P < 0.05$ 1-way RMA, Fig. 1B,C, Table 2A). Similar to NBI treatment, the peak amplitude and rise time ($P > 0.05$ paired Student's *t*-test) were not significantly affected, while the decay time course (τ) was significantly prolonged ($P < 0.05$ paired Student's *t*-test. Fig. 2B, Table 2A). The effects of α-helical $CRH_{(9-41)}$ (1 μM) were fully reversed following a >20 min wash period (99 ± 7% of CTRL, $n = 3$. Fig. 1D). Together, these data constitute the first demonstration that endogenous CRH enhances excitatory input to pyramidal cells in hippocampus, most likely through an interaction with CRHR1.

The reduced frequency and prolonged decay time of sEPSCs following inhibition of CRH signaling suggested possible presynaptic and postsynaptic mechanisms of action. To examine this possibility, we used 2 approaches. First, we characterized the properties of mEPSCs recorded from CA3 pyramidal cells (Table 1). Given that CRHR1 is the primary receptor for CRH within the hippocampus (Chen et al. 2000), we assessed the effect that bath application of NBI 30775 ([1 μM] CRHR1 selective antagonist) had upon the properties of these synaptic currents. Inhibition of CRHR1 signaling significantly reduced the frequency of mEPSCs recorded from CA3 pyramidal cells (71 ± 6% CTRL frequency, $n = 5$, $P < 0.05$ 1-way RMA, Fig. 1C, Table 2A), without influencing peak amplitude, rise time, or decay time course ($P > 0.05$ paired Student's *t*-test; Fig. 2C, Table 2A). Collectively these observations suggest that endogenous CRH has a positive effect on glutamate release in CA3 with no direct action upon the function of postsynaptic glutamate receptors. The second approach to localize the synaptic actions of CRH involved electron microscopy (EM). We have previously identified a postsynaptic location of CRH on dendritic spines (Chen et al. 2010). Here, we conducted immuno-gold EM

Table 1. Properties of mEPSCs, sEPSCs, and sIPSCs recorded from CA3 pyramidal cells

	mEPSCs ($n = 12$)	sEPSCs ($n = 29$)	sIPSCs ($n = 14$)
Peak amplitude (pA)	−39 ± 2	−50 ± 2*	70 ± 8
Rise time (ms)	1.7 ± 0.2	2.0 ± 0.1	2.0 ± 0.2
T50% (ms)	7.4 ± 0.7	7.9 ± 0.5	17.1 ± 0.7
τ (ms)	8.3 ± 0.5	8.8 ± 0.5	19.4 ± 0.7
Frequency (Hz)	1.0 ± 0.2	3.9 ± 0.6*	14.4 ± 1.6

*$P < 0.05$ unpaired Student's *t*-test versus mEPSCs.

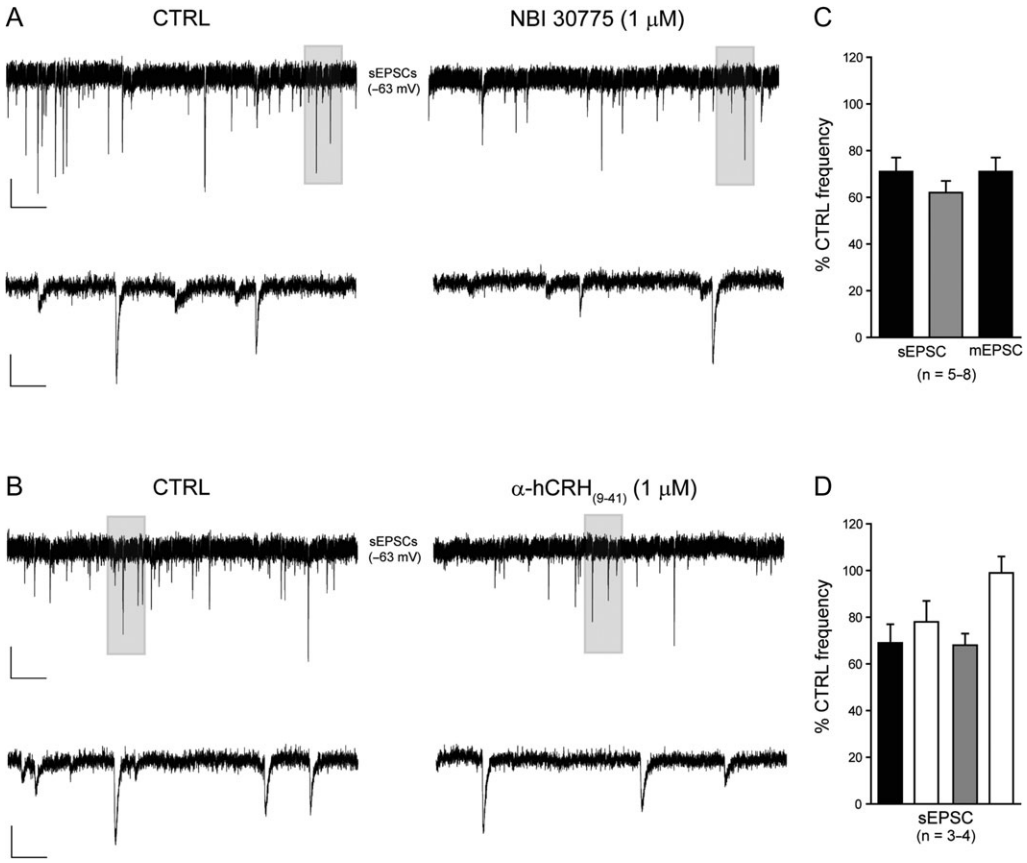

Figure 1. The frequency of EPSCs is reduced following inhibition of the CRHR1. Illustrated are sections (10 s) of whole-cell voltage clamp recordings of sEPSCs in the absence (left panel) and presence (right panel) of NBI 30775 (1 μM, *A*) and α-hCRH$_{(9-41)}$ (1μM, *B*) recorded from representative CA3 pyramidal cells. A section (shaded, 1 s) is shown on an expanded time scale. Scale bars y = 25 pA, x = 1 and 0.1 s for top and bottom traces, respectively. (*C*) Bar graph summarizing the effect of NBI 30775 (1 μM, black) and α-hCRH$_{(9-41)}$ (1μM, gray) upon the frequency synaptic currents recorded from CA3 pyramidal cells. (*D*) Bar graph summarizing the effect of washout (white) upon the NBI 30775 (1 μM, black) and α-hCRH$_{(9-41)}$ (1μM, gray) induced reduction in the frequency of sEPSCs recorded from CA3 pyramidal cells.

Table 2. Summary of the effects of the CRHR1 antagonists NBI 30775 (1 μM) and α-helical CRH$_{(9-41)}$ (1 μM) upon the properties of excitatory (A) and inhibitory (B) synaptic currents recorded from CA3 pyramidal cells

A	mEPSCs (n = 5)		sEPSCs (n = 8)		sEPSCs (n = 5)	
	CTRL	NBI (1 μM)	CTRL	NBI (1 μM)	CTRL	CRH$_{(9-41)}$ (1 μM)
Peak amplitude (pA)	−40 ± 4	−44 ± 7	−54 ± 4	−55 ± 3	−46 ± 6	−51 ± 6
Rise time (ms)	1.3 ± 0.2	1.3 ± 0.3	2.0 ± 0.2	2.3 ± 0.3	1.8 ± 0.3	2.0 ± 0.4
T50% (ms)	7.1 ± 1.0	7.5 ± 0.7	7.1 ± 0.4	9.3 ± 0.9*	6.6 ± 1.2	7.9 ± 1.5
τ (ms)	8.0 ± 1.2	7.6 ± 1.1	8.4 ± 0.6	11.2 ± 1.3*	6.6 ± 1.0	8.0 ± 1.4*
Frequency (Hz)	1.2 ± 0.4	1.0 ± 0.4*	3.4 ± 0.7	2.4 ± 0.5*	4.6 ± 1.4	2.8 ± 1.0*

B	sIPSCs (n = 4)		sIPSCs (n = 3)	
	CTRL	NBI (1 μM)	CTRL	CRH$_{(9-41)}$ (1 μM)
Peak amplitude (pA)	74 ± 17	112 ± 32	56 ± 17	53 ± 14
Rise time (ms)	2.7 ± 0.5	2.6 ± 0.7	1.5 ± 0.3	1.7 ± 0.5
T50% (ms)	19.2 ± 0.2	17.3 ± 1.0	15.0 ± 1.4	17.2 ± 1.0
τ (ms)	20.0 ± 1.3	19.8 ± 0.6	17.8 ± 1.1	19.3 ± 1.6
Frequency (Hz)	9.8 ± 2.0	10.4 ± 1.8	13.2 ± 2.7	12.4 ± 1.7

*$P < 0.05$ paired Student's t-test versus CTRL.

immunohistochemistry of the CRHR1 on mouse hippocampal sections, focusing on CA3. We found clear evidence for the presence of the receptor on both presynaptic and postsynaptic elements of excitatory synapses in the CA3 stratum oriens (Fig. 2*D*,*E*). Together, the electrophysiological and neuroanatomical data converged to support both presynaptic and postsynaptic actions of endogenous CRH on excitability within the hippocampal network.

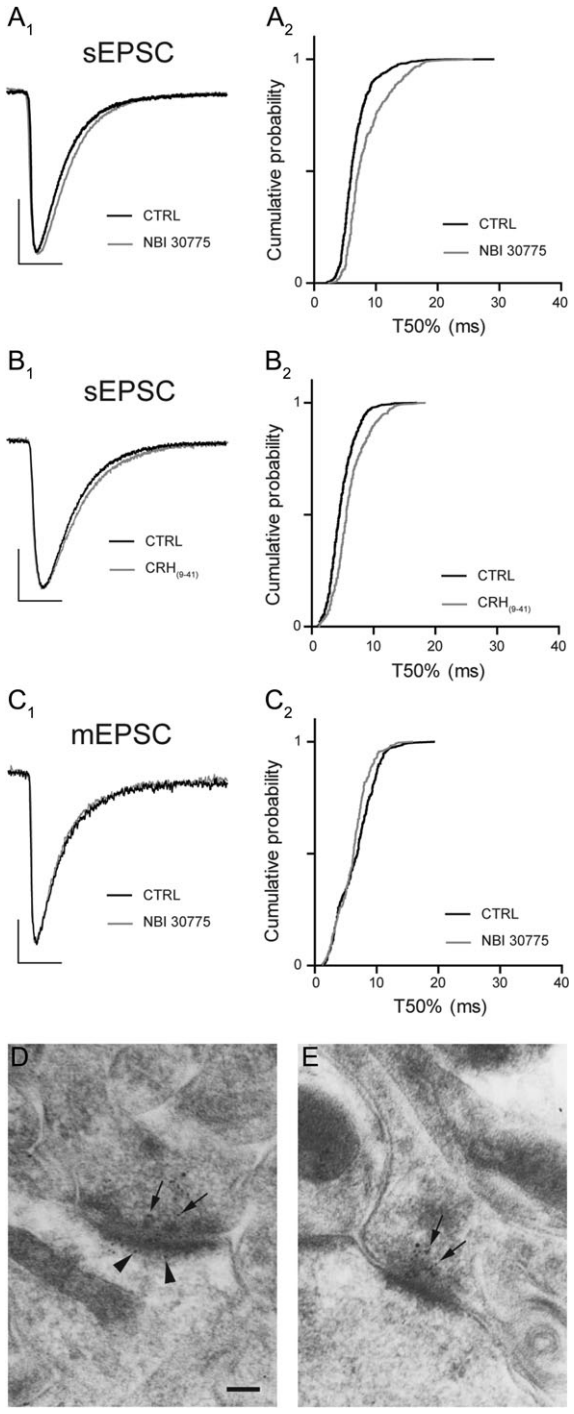

Figure 2. Inhibition of CRHR1 has no significant effect upon the properties of postsynaptic glutamate receptors. Superimposed normalized ensemble averages of sEPSCs recorded from a representative CA3 pyramidal neuron before (black) and after (gray) bath application of NBI 30775 (1 μM, A_1) and α-hCRH$_{(9-41)}$ (1 μM, B_1). Note the modest prolongation of the decay time course for both. Scale bar y = 20 pA, x = 10 ms. Cumulative probability plot of T50% decay time of all sEPSCs recorded from CA3 pyrmaidal cells before (black) and after (gray) bath application of NBI 30775 (1 μM, A_2) and α-hCRH$_{(9-41)}$ (1 μM, B_2). Superimposed normalized ensemble averages of mEPSCs recorded from a representative CA3 pyramidal neuron before (black) and after (gray) bath application of NBI 30775 (1 μM, C_1). Note the lack of effect upon the decay time course for both. Scale bar y = 10 pA, x = 10 ms. Cumulative probability plot of T50% decay time of all mEPSCs recorded from CA3 pyrmaidal cells before (black) and after (gray) bath application of NBI 30775 (1 μM, C_2). Representative electron mircrographs of asymmetric synapses in the stratum oriens of CA3 illustrating the expression of CRHR1 at pre- (arrows) and postsynaptic (arrowheads) sites within a single synapse (*D*) and within the presynaptic terminal (arrows) only (*E*). Scale bar = 100 nm.

Inhibition of CRHR1 has No Effect Upon Inhibitory Transmission in CA3 Pyramidal Cells

Having established that endogenously released CRH enhances phasic excitatory transmission, we next examined whether inhibitory transmission was additionally modulated by this peptide. Initial experiments characterized the properties of sIPSCs recorded from CA3 pyramidal cells at the holding potential for $E_{glutamate}$ (0 mV, Table 1), preserving the integrity of the local network. Bath application of NBI 30775 (1 μM) or α-helical CRH$_{(9-41)}$ (1 μM) had no significant effect upon any of the properties of these $GABA_A$ receptor ($GABA_AR$)-mediated events (Fig. 3A–C; Table 2B). We then examined the effects of blocking the CRH receptor on the function of specific $GABA_AR$ isoforms that are located at peri- and extra-synaptic sites where they mediate a persistent form of tonic inhibition (Farrant and Nusser 2005). Under our recording conditions, the bath application of the $GABA_AR$ antagonist, bicuculline (20 μM) attenuated all sIPSCs and induced a modest inward current (–7.0 ± 3.6 pA, $n = 7$) and significant reduction in the RMS (CTRL: 4.2 ± 0.6 pA, Bic: 2.8 ± 0.5 pA, $n = 7$, $P < 0.05$ paired Student's *t*-test, Fig. 3D,E). Inhibition of CRHR1 with NBI 30775 (1 μM) or with α-helical CRH$_{(9-41)}$ (1 μM) produced a modest, but nonsignificant (when accounting for temporal drift, see Methods) outward current (NBI: 18.8 ± 3.1 pA, $n = 4$; CRH$_{(9-41)}$: 11.2 ± 6.4 pA, $n = 3$) that was fully reversed following the application of bicuculline (Fig. 3E,F). No significant effect on the RMS was observed with either antagonist (CTRL: 5.7 ± 0.3 pA, NBI: 6.6 ± 0.7 pA, $n = 4$; CTRL: 3.5 ± 0.8 pA, CRH$_{(9-41)}$: 3.5 ± 1 pA, $n = 3$, $P > 0.05$ paired Student's *t*-test). These findings demonstrate that CRH released endogenously within hippocampal CA3 does not influence $GABA_AR$-mediated inhibition of pyramidal cells.

Endogenous CRH Reduces Action Potential Frequency and Prolongs I_{AHP}

Having established that endogenous CRH, via both presynaptic and postsynaptic sites, selectively enhances excitatory transmission onto CA3 pyramidal cells, we looked to identify any potential mechanism(s) that may underlie these observed actions of the peptide. Given that the frequency of glutamatergic transmission onto CA3 pyramidal cells is highly dependent upon action potential driven release (sEPSCs: 3.9 ± 0.6 Hz, $n = 29$; mEPSC: 1.0 ± 0.2, $n = 12$, $P > 0.05$ unpaired Student's *t*-test, Table 1) and previous studies have demonstrated that the application of exogenous CRH increased the frequency of action potentials (Aldenhoff et al. 1983) we investigated the effect that inhibition of CRHR1 had upon the properties of spontaneous action potentials. Bath application of NBI 30775 (1 μM) produced a significant reduction in the action potential frequency (55 ± 7% CTRL, $n = 4$, $P < 0.05$ 1-way RMA, Fig. 4A,B, Table 3) with no significant effect upon the $V_{Membrane}$ or the action potential properties ($P > 0.05$ paired Student's *t*-test, Table 3). Previous studies have demonstrated that exogenously applied CRH increases action potential firing, at least partially, through the inhibition of Ca^{2+}-dependent K^+-channels that contribute to the generation of I_{AHP} (Aldenhoff et al. 1983; Haug and Storm 2000). Under our recording conditions, we were unable to detect any significant effect of inhibiting CRHR1 upon the I_{AHP} associated with spontaneous action potentials, although a (nonsignificant) prolongation of the I_{AHP}

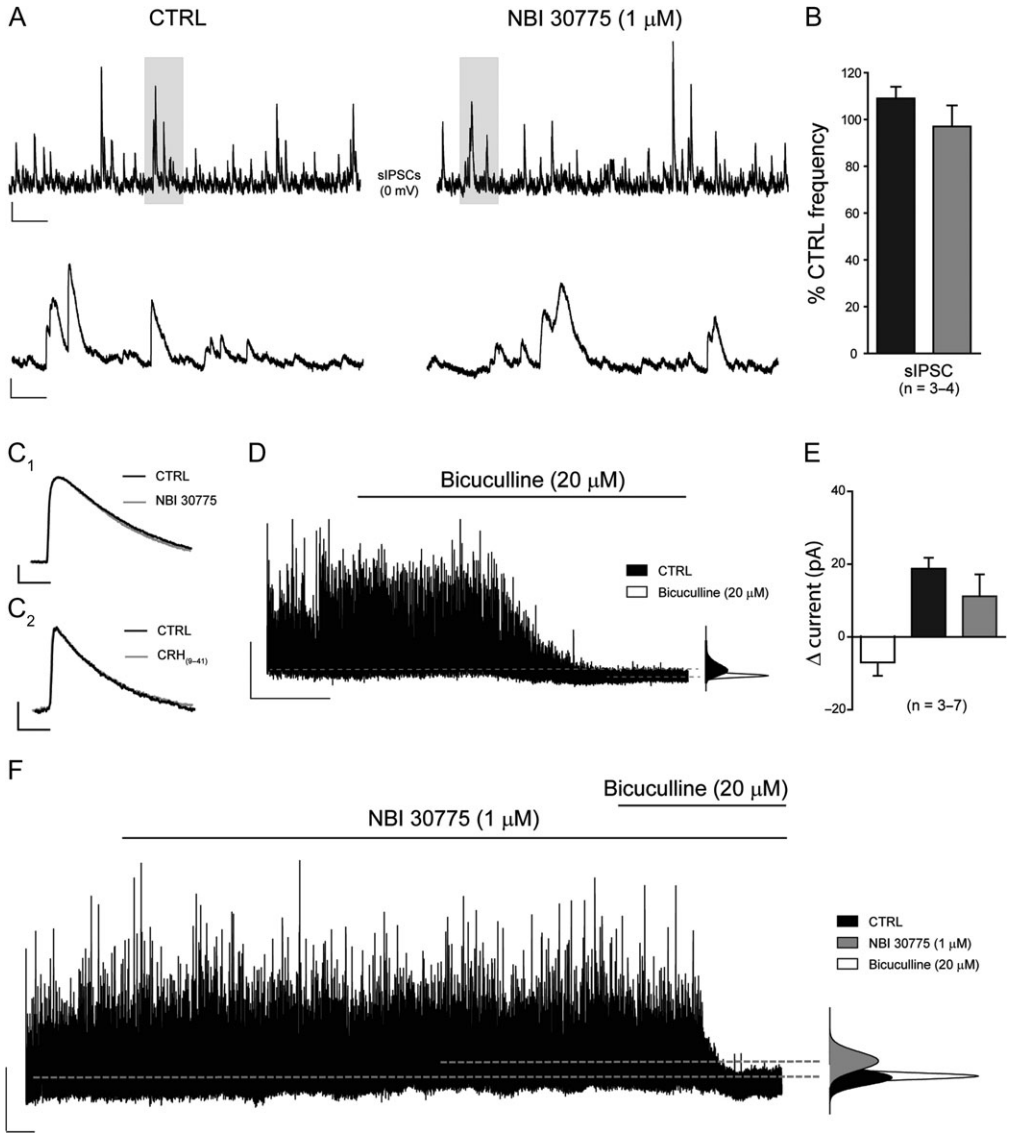

Figure 3. Inhibitory transmission is unaffected following treatment with the CRHR1 antagonists NBI 30775 and α-hCRH$_{(9-41)}$. Illustrated are sections (10 s) of whole-cell voltage clamp recordings of sIPSCs in the absence (left panel) and presence (right panel) of NBI 30775 (1 μM, *A*) recorded from a representative CA3 pyramidal cell. A section (shaded, 1 s) is shown on an expanded time scale. Scale bars y = 50 pA, x = 1 and 0.1 s for top and bottom traces, respectively. (*B*) Bar graph summarizing the effect of NBI 30775 (1 μM, black) and α-hCRH$_{(9-41)}$ (1 μM, gray) upon the frequency of sIPSCs. Superimposed normalized ensemble averages of sIPSCs recorded from a representative CA3 pyramidal neuron before (black) and after (gray) bath application of NBI 30775 (1 μM, C_1) and α-hCRH$_{(9-41)}$ (1 μM, C_2). Scale bar y = 20 pA, x = 10 ms. (*D*) Representative trace of whole-cell voltage-clamp recording made from a CA3 pyramidal cell. Bath application of the $GABA_AR$ antagonist bicuculline (20 μM) produced an inward current and an associated decrease in the RMS noise. The broken lines indicate the mean holding currents under each condition and the corresponding all points histograms (right) illustrate graphically any change in holding current associated with drug treatment. Scale bars y = 50 pA, x = 60 s. (*E*) Bar graph summarizing the effect of bicuculline (20 μM) and the CRHR1 antagonists, NBI 30775 (1 μM) and α-hCRH$_{(9-41)}$ (1 μM) upon the mean holding current of CA3 pyramidal cells. (*F*) Representative trace illustrating that the CRHR1 selective antagonist, NBI 30775 (1 μM), produces a modest outward current that is fully reversed following co-application of bicuculline (20 μM). The broken lines indicate the mean holding currents under each condition and the corresponding all points histograms (right) illustrate graphically any change in holding current associated with drug treatment. Scale bars: y = 50 pA, x = 60 s.

decay time (T50%) was observed in 3 out of 4 cells recorded (35 ± 23% CTRL). Eliciting an I_{AHP} with a brief depolarizing step (see Methods) resulted in a significant prolongation of the decay time (as described by the τ_W) following the bath application of NBI 30775 (1 μM, Fig. 4*C*,*D*, Table 3). No significant effect upon the peak amplitude or rise time of these currents was observed (Table 3). Collectively, these data suggest that endogenously released CRH increases action potential frequency, at least in part through a reduction in I_{AHP} decay time, an effect that likely contributes to the enhanced glutamatergic transmission (i.e., sEPSC frequency) onto CA3 pyramidal cells.

Endogenous CRH Modulates CA3 Network Activity

We next examined the functional significance of augmented glutamatergic drive by endogenous CRH on an intra-hippocampal network. SPWs are a form of intrinsic network activity (i.e., they do not require external stimulation) believed to be important in memory consolidation (Buzsaki 1989, 2015). They occur, with the same essential characteristics as found in vivo, spontaneously in slices prepared from the temporal hippocampus (Kubota et al. 2003) and are generated in CA3 with initiation dependent upon both excitatory and inhibitory transmission (Maier et al. 2003;

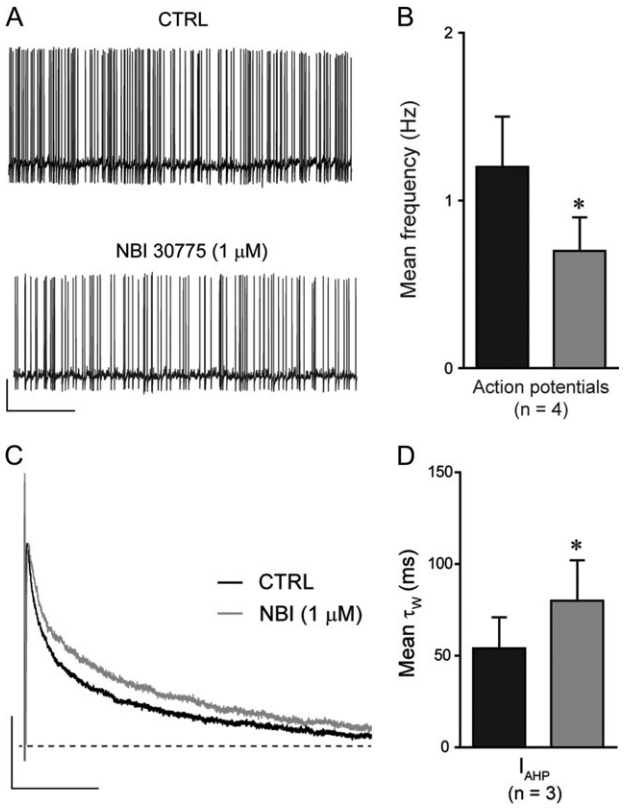

Figure 4. Inhibition of CRHR1 reduces the frequency of action potentials and prolongs the decay time course of I_{AHP}. (*A*) Illustrated sections (60 s) of whole-cell current-clamp recordings of spontaneous action potentials in the absence (top) and presence (bottom) of NBI 30775 (1 μM) recorded from a representative CA3 pyramidal cell. Scale bar y = 20 mV, x = 10 s. (*B*) Bar graph summarizing the mean action potential frequency in the absence (black) and presence (gray) of NBI 30775 (1 μM). *$P < 0.05$ paired Student's *t*-test versus CTRL. (*C*) Superimposed normalized ensemble averages of I_{AHP} recorded from a representative CA3 pyramidal neuron before (black) and after (gray) bath application of NBI 30775 (1 μM). Note the prolongation of the decay time course in the presence of NBI 30775. Scale bar y = 200 pA, x = 50 ms. (*D*) Bar graph summarizing the mean decay time (τ_W) of $I_{AHP's}$ in the absence (black) and presence (gray) of NBI 30775 (1 μM). *$P < 0.05$ paired Student's *t*-test versus CTRL.

Rex et al. 2009; Koniaris et al. 2011; Papatheodoropoulos and Koniaris 2011; Schlingloff et al. 2014). As described in earlier reports, SPWs recorded from the CA3 apical dendritic tree layer were negative-going potentials (Fig. 5*A*) that occurred irregularly and varied in their frequency across seconds-long recording epochs (e.g., 0.5–15 Hz). However, over 30 min or longer, mean baseline frequencies of SPW were consistent between slices (1.4 ± 0.2 Hz, $n = 11$). Intervals between individual SPWs were highly variable as illustrated by the histogram of IEI (Fig. 5*B*) and they resembled the distribution of sEPSCs recorded from CA3 pyramidal cells (Fig. 5*B* inset). The peak amplitude and area were also highly variable within slices (e.g., peak: −25 to −263 μV; area: −125 to −4250 μV.ms), but again comparable across cases (peak: −52.5 ± 2.0 μV; area: −867.3 ± 56 μV.ms, $n = 11$). Frequency and amplitude across slices were not correlated ($r = 0.18$). We further characterized the SPW waveform by quantifying the rise time (10–90%) and the decay time, described by the decay time constant τ, of the SPWs. The rising and decay phase of the SPW exhibited considerable variability within a slice (e.g., RT: 6–25 ms; τ: 10–250 ms), but were relatively consistent across slices (RT: 12 ± 0.6 ms; τ: 22 ± 3 ms, $n = 11$).

Table 3. Summary of the effects of the CRHR1 antagonist NBI 30775 (1 μM) upon the properties of spontaneous action potentials and evoked I_{AHP} recorded from CA3 pyramidal cells

	CTRL	NBI 30775 (1 μM)
Spontaneous action potentials ($n = 4$)		
Spike amplitude (mV)	75 ± 3	71 ± 4
Half-width (ms)	1.3 ± 0.1	1.4 ± 0.1
Rise time (ms)	0.6 ± 0.1	0.6 ± 0.1
Decay time (ms)	1.0 ± 0.1	1.1 ± 0.1
AHP amplitude (mV)	−8.4 ± 1.7	−7.2 ± 1.7
AHP T50%	13.4 ± 11	12.5 ± 10
Frequency (Hz)	1.2 ± 0.3	0.7 ± 0.2*
$V_{Membrane}$ (mV)	−71.2 ± 6	−71.1 ± 6
Evoked I_{AHP} ($n = 3$)		
Peak amplitude (pA)	326 ± 159	260 ± 92
Rise time (ms)	2.6 ± 2.2	1.2 ± 0.7
τ_W (ms)	54 ± 17	80 ± 22*

*$P < 0.05$ paired Student's *t*-test versus CTRL.

Bath application of NBI 30775 (1 μM), but not of vehicle (saline), significantly reduced the frequency of SPWs. Mean frequency for the baseline period, sampled in 2-min bins, was 1.57 ± 0.24 Hz and 1.11 ± 0.21 Hz for the 10 min span after 44 min of infusion with the antagonist ($P < 0.05$, paired Student's *t*-test, $n = 7$, Fig. 5*C*,*D*). Frequencies before and during application of NBI were highly correlated ($r = 0.909$), as expected for stable recording conditions. Moreover, there was no evidence of pre-post changes in SPW frequency in vehicle (saline) treated slices ($P > 0.20$ paired Student's *t*-test, $n = 4$, Fig. 5*C*,*D*). In contrast to its effects on frequency, NBI 30775 did not influence peak amplitude, area, rising phase or decay phase of SPWs ($P > 0.05$ paired Student's *t*-test, Fig. 5*E*–*G*, Table 4). Values for the 2 sampling periods separated by 44 min were again highly correlated ($r = 0.946$).

To assess the time course for NBI 30775's actions, we normalized the frequency values (2 min bins) for each slice to the mean of the pre-infusion baseline period and then plotted over time values. A statistically reliable effect ($P < 0.05$ 1-way RMA) was found at 10 min after the beginning of application and for all subsequent sampling periods (Fig. 5*C*). Given that subfusion was used, this constitutes a rapid onset of action for the antagonist. We interpret the result as indicating that released CRH rapidly acts to influence SPW frequency.

Modulating CA3 Pyramidal Cell Excitability Influences Simulated SPW Activity in a Hippocampal Model

To investigate potential causality between selective modulation of excitatory transmission by endogenous CRH and the generation of SPWs within the hippocampus CA3, we utilized a simulated DG-CA3-CA1 neuronal network (Supplementary Fig. 1*A* and Methods). We first confirmed the ability of the modified hippocampal simulation to generate SPWs in the dendritic cell layers of CA3 and CA1 (Supplementary Fig. 2*A*1-2, *B*1-2), and determined the nature of pyramidal cell and interneuron spiking (at the single-neuron level) that underlies these events (Supplementary Fig. 2*C*1-2, *D*1-2). The simulated firing rate was higher in CA1 pyramidal cells and interneurons in comparison to their CA3 counterparts, most likely due to amplification of CA3 output, associated with a high level of connectivity between CA3 pyramidal cells and CA1 neurons (Supplementary Fig. 2*B*). Consistent with experimental data (Rex et al. 2009), the strength of mossy fiber synapses (i.e., α_{syn}, see Methods) within our simulation greatly influenced the generation

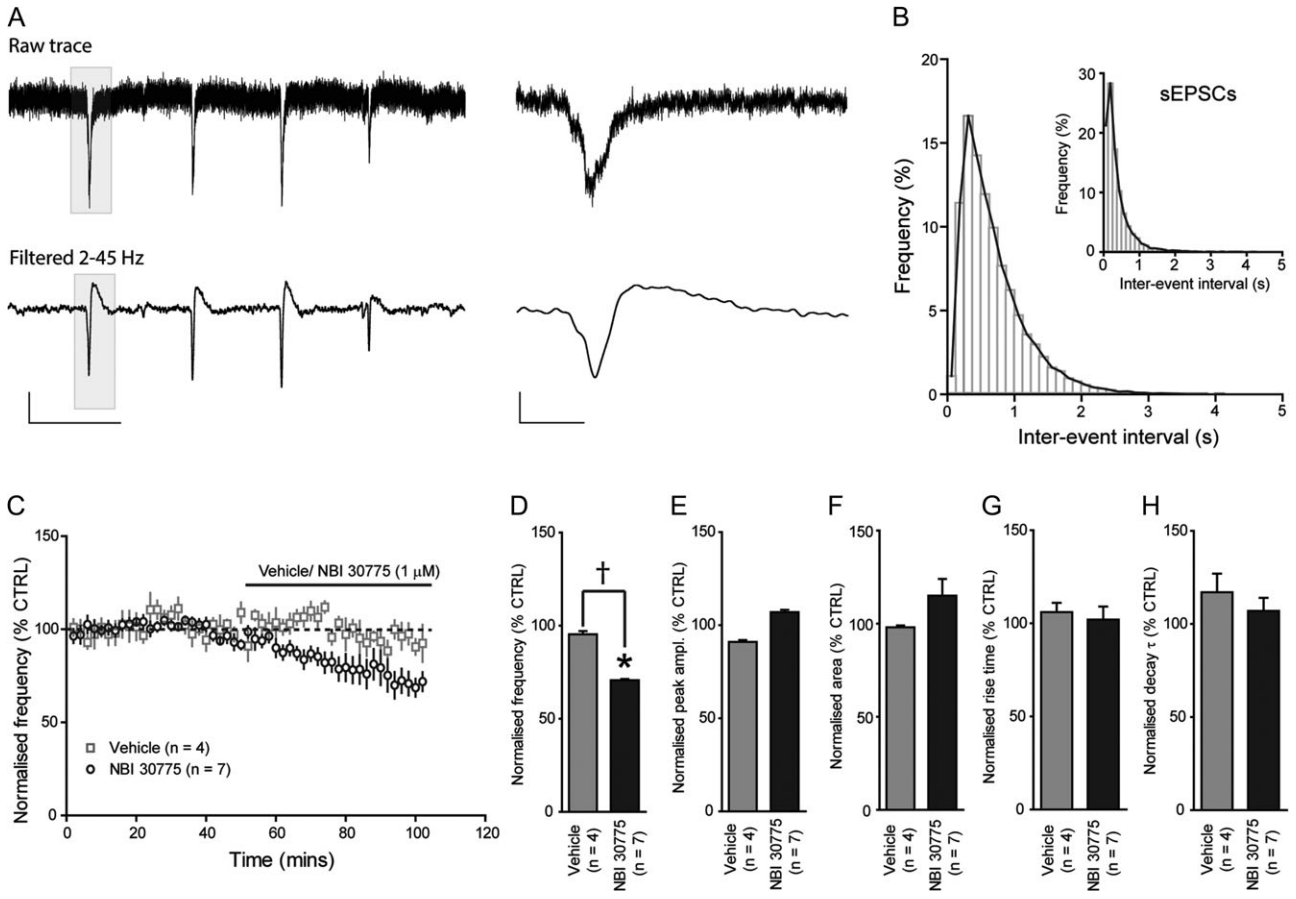

Figure 5. The CRHR1 antagonist NBI 30775 (1 μM) reduces the frequency of SPWs in the CA3. (*A*) Illustrated sections (5 s) of unfiltered (top) and filtered (bottom) extracellular recording of SPWs from the apical dendrites of the CA3 pyramidal cell layer. A section of each (shaded, 500 ms) is shown on an expanded time scale (right panel). Scale bars $y = 25\,\mu V$, $x = 1$ and 0.1 s for top and bottom traces, respectively. (*B*) Histogram of IEI of SPWs recorded under baseline conditions ($n = 11$). For comparison, the inset illustrates the IEI distribution of sEPSCs recorded under control conditions. (*C*) Summary graph depicting the time course of the effect of vehicle (saline) and NBI 30775 (1 μM) upon the frequency of SPWs recorded from the CA3. Bar graphs summarizing the effects of vehicle and NBI 30775 (1 μM) upon the frequency (*D*), peak amplitude (*E*), area (*F*), rise time (*G*), and decay τ (*H*) of SPWs (*$P < 0.05$ vs. CTRL 1-way RMA, †$P < 0.05$ saline vs. NBI 2-way RMA).

of SPWs. Furthermore, the degree of synchronization of a threshold level of mossy fiber input (20% of DG cell firing) was found to profoundly influence the probability of SPW initiation. Specifically, 20% of DG cells firing over a 10, 50, 100, and 200 ms period resulted in a 23%, 7%, 3%, and 0% chance of a SPW occurring within the CA3, respectively.

Because our electrophysiological data suggested that endogenously released CRH enhances glutamatergic transmission onto CA3 pyramidal cells and augments SPW frequency, we focused on examining if a change in the frequency of excitatory synaptic transmission onto these neurons influences SPW generation in our hippocampal simulation. Because the hippocampal model has no cortical inputs (i.e., no input from entorhinal cortex), we modulated the frequency of EPSCs onto CA3 pyramidal cells by manipulating the nature of the output from the DG. Increasing the frequency of DG output resulted in an activity-dependent increase in the frequency of EPSCs in individual CA3 pyramidal cells (Fig. 6*A*,*B*). Remarkably, this effect was associated with a greater incidence of SPWs in both CA3 and CA1 (Fig. 6*C*,*D*). Thus, the model faithfully recapitulated the electrophysiological observation, where we find endogenous CRH increases both the frequency of EPSCs and the occurrence of SPWs, and thus provides a causal relationship between the frequency of excitatory currents onto CA3 pyramidal cells and incidence of SPW. Additionally, increasing the frequency of EPSCs on to CA3 pyramidal neurons via a second manipulation (enhancing the scaled synaptic strength; Fig. 7*A*,*B*, see Methods), also resulted in augmented SPW frequency in both regions (Fig. 7*C*,*D*). This effect was likely associated with a reduction in the probability of SPW generation as reducing the scaled synaptic strength (from 1.5 to 1.4 a.u.) completely attenuated the likelihood of SPW initiation at threshold levels

Table 4. Summary of the effects of saline and NBI 30775 (1 μM) treatment upon the properties of SPWs recorded from the apical dendrites of CA3 pyramidal cells

	SPWs ($n = 4$)		SPWs ($n = 7$)	
	CTRL	Saline	CTRL	NBI (1 μM)
Peak amplitude (μV)	−49 ± 2.4	−45 ± 2.5	−55 ± 3.0	−59 ± 6.9
Rise time (ms)	12.8 ± 0.9	13.8 ± 1.1	11.6 ± 0.8	11.9 ± 0.9
Area (μV.ms)	−838 ± 54	−825 ± 44	−884 ± 68	−1030 ± 146
τ (ms)	27.1 ± 5.4	33.0 ± 9.1	19.6 ± 2.7	20.9 ± 3.2
Frequency (Hz)	1.1 ± 0.1	1.0 ± 0.1	1.6 ± 0.3	1.1 ± 0.2*

*$P < 0.05$ paired Student's *t*-test versus CTRL.

(20% DG cells firing) and was irrespective of input synchrony to CA3 pyramidal cells.

To probe if augmentation of SPW generation was specifically associated with phasic excitatory transmission, and as such add specificity to our observed effects of CRH, we used the hippocampal model to examine how the amplitude of a residual excitatory current in CA3 pyramidal cells influenced these events. Interestingly, increasing the amplitude of such a depolarizing current in CA3 pyramidal cells had no effect upon the frequency of SPWs in the CA3 (Fig. 8A,B), but did cause a reduction in the amplitude of these events (Fig. 8A bottom). The reduced amplitude and lack of effect upon the frequency of SPWs in the CA3 array likely results from a desynchronization of pyramidal cell spiking as illustrated by the raster plot (Fig. 8A top). Indeed, although the number of pyramidal cell clusters does increase in an input-dependent manner (Fig. 8D_1), the size of these clusters does not change in response to the residual current amplitude (Fig. 8D_2), an effect that likely explains the qualitative increase in the small SPW-like events observed in the CA3 (Fig. 8A bottom). Paradoxically, increasing the residual excitatory current in CA3 pyramidal cells did result in an increase in the SPW frequency in the CA1 (Fig. 8B,C). This effect likely result from the strong amplification of the signal generated by the small clusters of pyramidal cells spiking in CA3 (Fig. 8A) through the Schaeffer collateral connection to the CA1 array (Supplementary Fig. 1 & see Methods).

Collectively, these findings from modeling and electrophysiological studies, demonstrate that neuron- or indeed-synapse specific modulation of phasic transmission by an endogenous peptide, in this case CRH, can significantly influence information transfer through the hippocampal network. Notably, the hippocampal simulations reveal that the effects that pyramidal cell excitability has upon network processes in this region depend on the nature of the modulated excitatory drive (i.e., residual current and transient synaptic currents).

Discussion

The current study provides the first evidence that modulation of synaptic transmission at the single-neuron level by an endogenously released neuropeptide influences complex network processes within the hippocampus. Because acute stress rapidly releases CRH (Chen et al. 2004b, 2010), the effects of this peptide upon synaptic physiology and SPW activity that we describe here are of particular relevance to the well described stress-induced alterations of hippocampal memory processes.

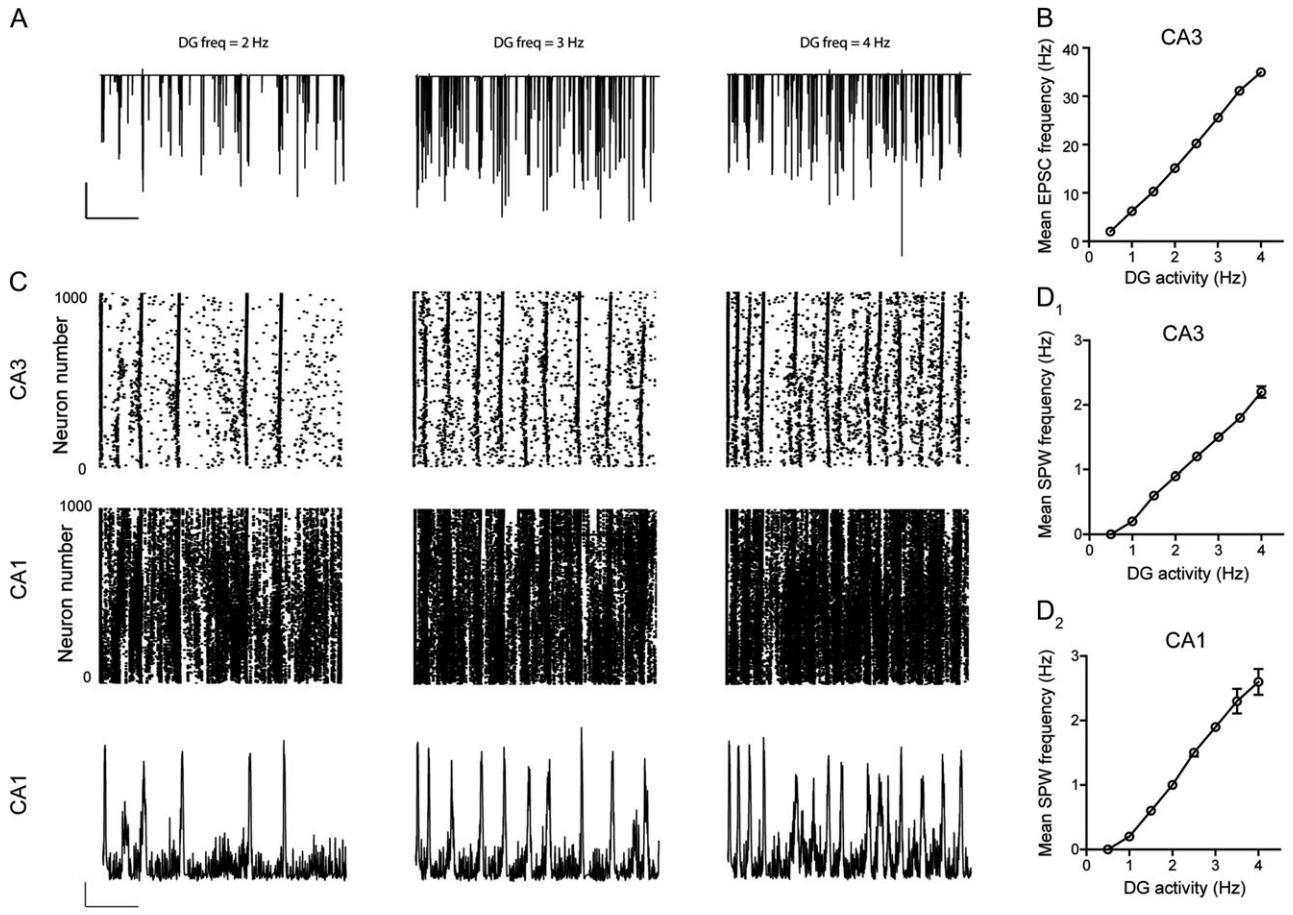

Figure 6. DG activity influences the frequency of EPSCs onto CA3 pyramidal cells and the generation of SPWs. (*A*) Representative sections (5 s) of simulation illustrating the frequency of EPSCs in CA3 pyramidal cells at increasing levels of DG activity. Scale bars y = 20 nA, x = 1 s. (*B*) Graph illustrating the mean frequency of simulated EPSCs onto CA3 pyramidal cells versus DG activity. (*C*) Raster plots of spike times for each CA3 and CA1 pyramidal cell (whole array) in the simulated network at 3 values of DG activity. Corresponding simulated SPWs generated in the CA1 for each value (bottom). Scale bars y = 10 mV, x = 1 s. Mean frequency of SPWs in CA1 (D_1) and CA3 (D_2) versus level of DG activity.

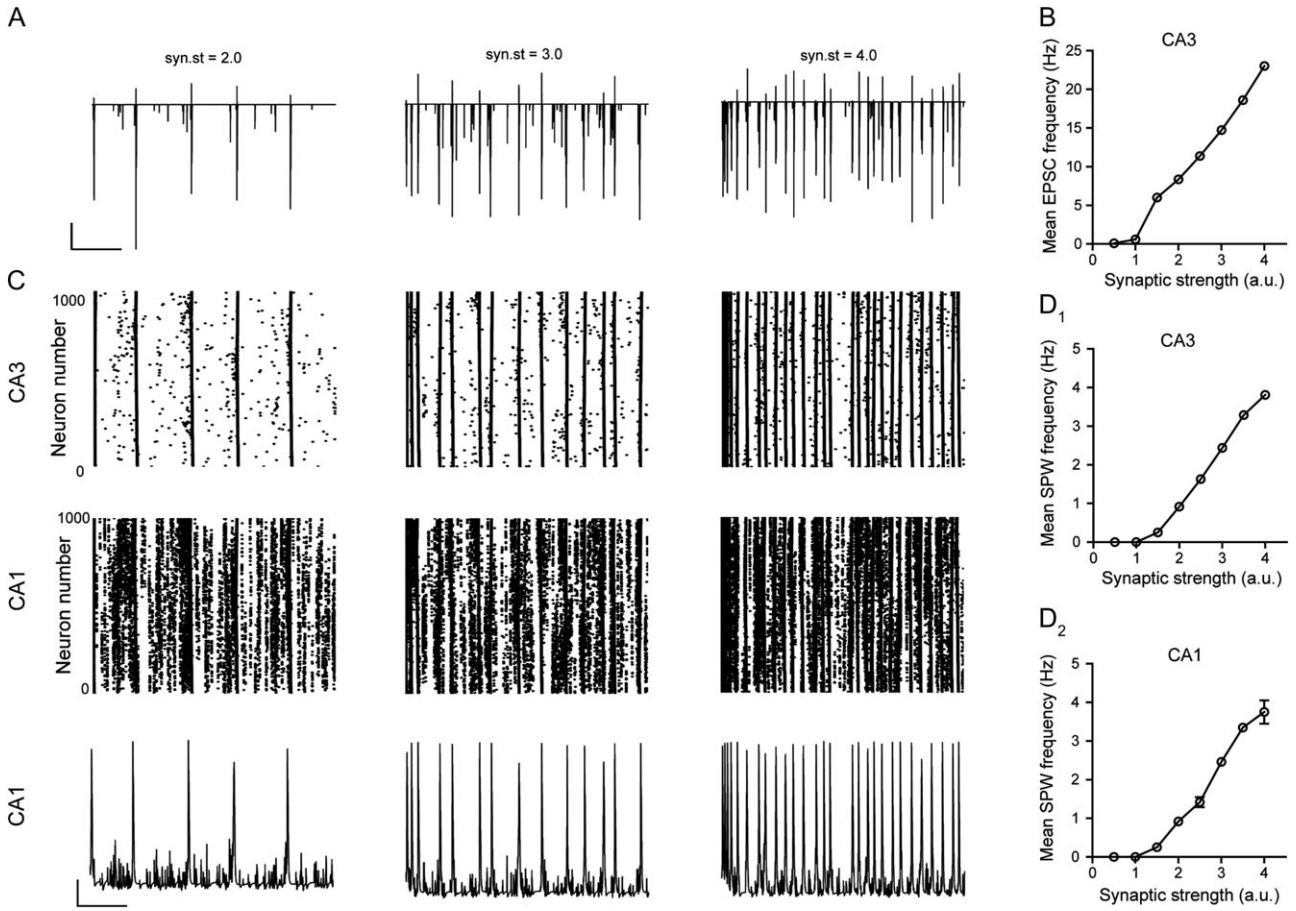

Figure 7. The strength of excitatory synaptic conductance onto CA3 pyramidal cells influences the frequency of EPSCs and the generation of SPWs. (*A*) Representative sections (5 s) of simulation illustrating the frequency of EPSCs in CA3 pyramidal cells at increasing levels of scaled synaptic strength onto these cells. Scale bars y = 20 nA, x = 1 s. (*B*) Graph illustrating the mean frequency of simulated EPSCs onto CA3 pyramidal cells versus scaled synaptic strength. (*C*) Raster plots of spike times for each CA3 and CA1 pyramidal cell (whole array) in the simulated network at 3 values of scaled synaptic strength. Corresponding simulated SPWs generated in the CA1 for each value (bottom). Scale bars y = 10 mV, x = 1 s. Mean frequency of SPWs in CA1 (D_1) and CA3 (D_2) versus scaled strength of excitatory synapses onto CA3 pyramidal cells.

Endogenous CRH Alters the Excitatory/Inhibitory Balance of CA3 Pyramidal Cells

Inhibition of CRHR1 with NBI 30775 significantly reduced the frequency of both sEPSCs and mEPSCs suggesting that endogenous CRH (directly and/ or indirectly) increases glutamate release from presynaptic terminals. The bath application of the nonselective CRHR antagonist α-helical $CRH_{(9\text{-}41)}$, a structurally and mechanistically distinct compound, produced a similar reduction in the frequency of sEPSCs, which (given the paucity of CRHR2 expression within the hippocampus [Joels and Baram 2009]), suggests that the effects of CRH are likely mediated by the CRHR1. Exogenous CRH increases the excitability of individual and populations of pyramidal cells (Aldenhoff et al. 1983; Smith and Dudek 1994; Hollrigel et al. 1998), most likely through the inhibition of Ca^{2+}-dependent (SK) and A-type K^+ channels (Haug and Storm 2000; Kratzer et al. 2013). Consistent with these previous findings, the excitability of CA3 pyramidal cells was reduced following inhibition of CRHR1, and this reduction in action potential frequency was mediated, at least in part, by a potentiation of the decay time course (τ_W) of I_{AHP}. The elicited I_{AHP} is likely comprised of both BK- and SK-mediated currents and as such further experiments using pharmacological tools are required to determine the precise molecular target of endogenous CRH. However, the observation that inhibition of CRHR1 appeared to preferentially prolong the slow τ_2 component of the τ_W (CTRL: 152 ± 17 ms, NBI: 239 ± 15 ms, $n = 3$, $P = 0.085$) suggests that the SK channel that mediates the medium and slow I_{AHP} may be the target. Although not investigated in the current study, inhibition of A-type K^+ channels by endogenous CRH may also contribute to the observed reduction in sEPSC frequency as such an effect of the peptide may linearize the summation of temporally distinct synaptic events originating in proximal and distal dendrites (Urban and Barrionuevo 1998), likely influencing the input–output relationship of these neurons. Thus, the inhibition of CRHR1, located on pyramidal cell dendrites (Chen et al. 2010), results in the reduced intrinsic excitability (i.e., prolongation of I_{AHP}) of these neurons and may additionally impair the integration of their synaptic inputs. Either effect (individually or combined) will result in a net reduction in spiking by the densely interconnected neurons of field CA3 (Swanson et al. 1978; Amaral and Witter 1989) and hence the significant reduction in the frequency of sEPSCs described here. While directly reducing the excitability of the associational system is an attractive mechanism for the observed effects following the inhibition of CRHR1, a decrease in release from mossy fiber inputs may also contribute. Although it remains to be established whether CRHR1 is located on mossy

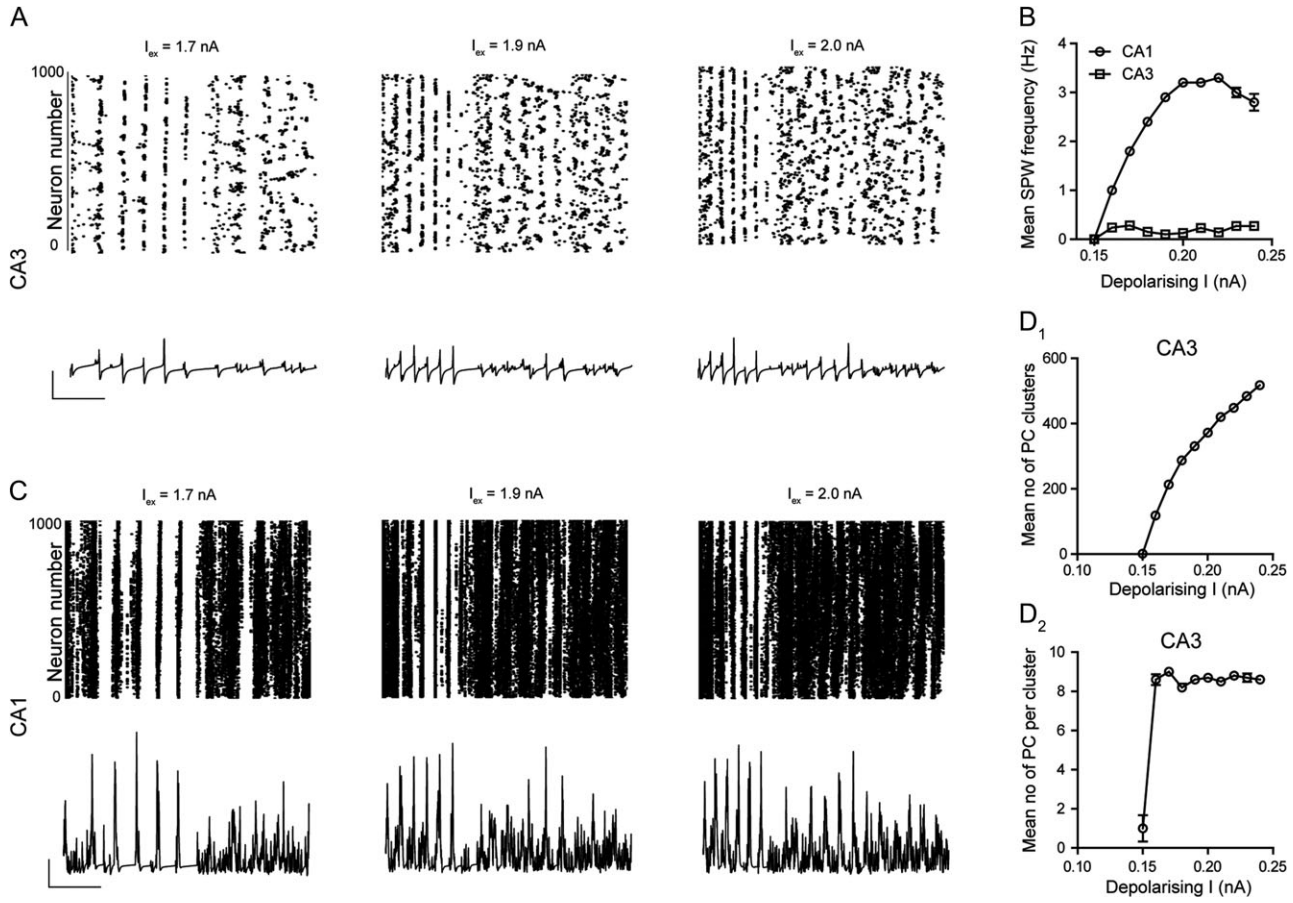

Figure 8. Depolarizing CA3 pyramidal cells desynchronizes CA3 pyramidal cell firing and reduces SPW amplitude. (*A*) Raster plots (top) of spike times for each CA3 pyramidal cell (whole array) in the simulated network at 3 values of depolarizing current into CA3 pyramidal cells. Corresponding simulated SPWs (below) generated from 55 cells for each depolarizing current value. Note the decrease in synchronous pyramidal cells spiking in the raster plots accompanied by a reduction in the amplitude of SPWs generated in CA3. Scale bars y = 10 mV, x = 1 s. (*B*) Mean frequency of SPWs in the CA1 and CA3 versus depolarizing current onto CA3 pyramidal cells. (*C*) Raster plots (top) of spike times for each CA1 pyramidal cell (whole array) in the simulated network at 3 values of depolarizing current into CA3 pyramidal cells. Corresponding simulated SPWs (below) generated from 55 cells for each depolarizing current. Note that in comparison to CA3, the SPW amplitude appears less reduced. Scale bars y = 10 mV, x = 1 s. Graph illustrating the mean number of clusters of spiking CA3 pyramidal cells (D_1) and the mean number of pyramidal cells per cluster (D_2) in response to increasing depolarizing current injection to these neurons.

fiber boutons, the receptor is expressed in DG cells (Chen et al. 2000), thus providing the anatomical basis for the potential modulation of action potential driven release.

In addition, inhibition of CRHR1 with NBI 30775 prolonged the decay time course (both T50% and τ values) of CA3 pyramidal cell sEPSCs (a significant prolongation of τ by α-helical $CRH_{(9\text{-}41)}$), but not mEPSCs. This finding is somewhat paradoxical, as prolongation of the decay time of synaptic currents is often associated with "spill over" of neurotransmitter as a result of increased frequency. However, the nature of vesicular release (i.e., synchronous or asynchronous) can also significantly influence the postsynaptic response due to alterations in neurotransmitter concentrations at the synapse (Rudolph et al. 2015). Although the precise mechanism(s) responsible for modulating vesicular release remain unknown, a role for presynaptic Ca^{2+} has been suggested (Kaeser and Regehr 2014). Whether, CRH does indeed influence the nature of vesicular release, for example through alterations in the temporal summation of spatially distinct synaptic inputs (Urban and Barrionuevo 1998), or by directly modulating Ca^{2+} influx to the presynaptic terminal (Takuma et al. 1994; Ritchie et al. 1996) remains to be established.

Blocking CRHR1 also reduced the frequency of mEPSCs, suggesting a presynaptic and action-potential independent mode of action. The mechanisms governing stochastic glutamate release in the CA3 remain to be fully elucidated (Scanziani et al. 1992), although this process may be regulated by both Ca^{2+}-dependent and -independent mechanisms (Kaeser and Regehr 2014; Schneggenburger and Rosenmund 2015). CRH has been shown to modulate calcium influx and, hence cytosolic levels, in a number of different cell types (Takuma et al. 1994; Ritchie et al. 1996) raising the possibility that this peptide may influence glutamatergic vesicle release probability, via calcium-dependent or -independent mechanisms. Such an argument implies that CRHR1s are found on a significant population of terminals. In support of this notion, EM demonstrated CRHR1 at presynaptic locations. Figure 2 shows presynaptic CRHR1 in stratum oriens of CA3, and additional presynaptic sites are likely, based on our electrophysiological studies in stratum pyramidale. Our finding of a novel role of presynaptic CRHR1 in the hippocampus are in accord with established roles of presynaptic CRHR1 in, for example, the central nucleus of the amygdala (Bajo et al. 2008). It should be noted that the observed effect upon the frequency of mEPSCs was not reported following the application of

exogenous CRH (Hollrigel et al. 1998). Such a discrepancy between the 2 studies may result from different recording conditions, such as the lack of $GABA_AR$ antagonists in the present study, and/or from species differences (i.e., mouse vs. rat). Blocking CRHR1 with NBI 30775 did not influence the decay time course (both T50% and τ values) of mEPSCs, suggesting that CRH is unlikely to influence AMPA receptor function per se; note also that this result is in line with the hypothesis that broadening of sEPSCs described above is likely a result of the desynchronization of action-potential driven multi-vesicular release. Thus, it is probable that CRH increases glutamate release on to CA3 pyramidal cells by both enhancing intrinsic neuronal excitability (i.e., action potential driven release) and through a direct action at presynaptic sites. However, given that inhibition of CRHR1 reduces action potential frequency, in part via a prolongation of I_{AHP}, and the frequency of EPSCs recorded from CA3 pyramidal cells is highly dependent upon action potential driven release (see Table 1 for mEPSC vs. sEPSC frequency) it would seem plausible that CRH exerts the majority of its effects via an increase in action potential driven release following the activation of postsynaptic CRHR1. Future studies using floxed CRH and CRHR1 mice may allow specific neuronal populations (expressing either CRH or CRHR1) to be functionally manipulated (e.g., using DREADDs or channel rhodopsin) to further elucidate the mechanism(s) of release and the precise functional actions of the endogenous peptide.

In contrast to actions on excitatory transmission, endogenous CRH appears to have no effect upon inhibitory synaptic transmission onto CA3 pyramidal cells, because treatment with NBI 30775 or α-helical $CRH_{(9\text{-}41)}$ had no significant effect upon any of the properties of sIPSCs (Table 2B). However, given the complex nature of the inhibitory network, along with the specific spatial and temporal pattern of pyramidal cell innervation associated with each class of interneuron (Klausberger and Somogyi 2008), we cannot rule out subtle changes associated with CRH modulating synaptic inputs from specific types of interneuron(s). In addition, under our recording conditions, inhibition of CRH had no significant effect upon the function of peri- or extra-synaptic $GABA_ARs$ responsible for mediating an inhibitory tonic conductance that contributes to the regulation of neuronal excitability (Farrant and Nusser 2005).

Collectively, these findings suggest that the constitutive release of CRH within the hippocampus enhances excitatory drive onto CA3 pyramidal cells while having no significant effect upon inhibitory transmission.

Endogenous CRH Increases SPW Frequency: Role of Excitatory/Inhibitory Balance?

The finding that CRH increases communication between CA3 neurons predicts that the peptide normally serves to enhance network level phenomena in that region. SPWs are a well-characterized example of the coordinated operation of CA3 cells acting through their unusually dense associational projections (Buzsaki 1986; Kubota et al. 2003). A CRHR1 antagonist caused a clear decrease in the incidence of SPWs; this finding constitutes the first evidence that endogenous CRH modulates the output of complex circuitry in the cortical telencephalon. Notably, exogenous CRH (100 nM) has recently been shown to have no effect upon the frequency of SPWs recorded from CA1 pyramidal cell layer (Caliskan et al. 2015). This apparent discrepancy points to the likely possibility that continuous stimulation of CRH receptors does not reproduce effects found with the presumably constrained and pulsatile or discrete release of local peptide.

The initiation of SPWs requires both excitatory and inhibitory transmission, although a consensus on the precise mechanism remains to be established. A number of studies have highlighted the importance of increased excitatory transmission prior to SPW generation (Maier et al. 2003; Wu et al. 2005; Papatheodoropoulos 2008) with release from mossy fiber terminals being identified as an important trigger in the generation of these events (Rex et al. 2009). Inhibitory transmission, mediated by parvalbumin (PV)-expressing interneurons appears to be critical for organizing pyramidal cell spiking and, hence, SPW generation (Schlingloff et al. 2014), while pharmacological manipulation of phasic and tonic $GABA_AR$ function lends further support to a role for GABAergic transmission in the initiation of these events (Koniaris et al. 2011; Papatheodoropoulos and Koniaris 2011). Our electrophysiological findings suggest that the selective enhancement of excitatory transmission onto CA3 pyramidal cells by an endogenous neuropeptide, with no effect upon $GABA_AR$ function, is sufficient to increase the likelihood of SPW initiation. Consistent with such a hypothesis, increasing the frequency of sEPSCs onto CA3 pyramidal cells resulted in an increase in the occurrence of SPWs in a simulated hippocampal network. Thus, our electrophysiological and hippocampal simulation data indicate that an increase in excitatory synaptic transmission onto CA3 pyramidal cells, most likely incorporating mossy fiber and associational synapses, results in an increased incidence of SPWs. Whether the generation of SPWs is influenced more strongly by modulation of a specific synapse (i.e., mossy fiber and axon collaterals) remains to be established. Interestingly, data from our hippocampal simulation suggests that the manner in which the excitability of CA3 pyramidal cells are modulated has a significant bearing on the network function. Thus, increasing the intrinsic excitability of CA3 pyramidal cells results in a desynchronization of principal cell spiking and the generation of SPW-like events in the CA3 that exhibit greatly reduced amplitude. An increase in the residual excitability of pyramidal cells likely shifts the balance in operating mode of these neurons toward integrators (i.e., away from coincidence detectors), an effect that will influence the synchrony transfer of inputs to these neurons (Ratte et al. 2013). Collectively, these observations demonstrate that enhanced synaptic transmission at a specific node(s) by an endogenous neuropeptide has the capacity to influence complex hippocampal network processes. This highlights a potentially common and important mechanism by which neuropeptides, of which many are expressed within the hippocampus, may influence hippocampal processing under physiological and pathophysiological states.

Potential Source and Release of Hippocampal CRH

Our data would suggest, at least to a degree, that constitutive CRH release and/or a lack of metabolism of this peptide within the hippocampus enhances excitatory synaptic transmission, which, given the "mis-matched" anatomy of the CRH synapse (Chen et al. 2010, 2012), most likely occurs via local diffusion of the peptide (van den Pol 2012). The heterogeneous population of CRH-expressing inhibitory interneurons located throughout the hippocampal regions (Chen et al. 2004b, 2015) make an attractive candidate as the source of CRH released within this brain region. Support for constitutive, intra-hippocampal CRH release from these interneurons comes from in vitro experiments using

organotypic slice cultures (i.e., lacking extra-hippocampal regions) where treatment with selective CRHR1 antagonists increased total dendritic length and arborization (Chen et al. 2004a, 2008). However, the possibility that CRH might reach hippocampal synapses from other brain regions (e.g., amygdala and hypothalamic PVN) cannot be ruled out. Support for the notion of an endogenous CRH "tone" within the hippocampus as a mechanism to modulate synaptic transmission comes from the central nucleus of the amygdala where the peptide was found to modulate GABAergic transmission (Herman et al. 2013).

While further studies are required to fully elucidate the source(s) of CRH release within the hippocampus, the distinct pharmacological profiles of the 2 antagonists used support the notion that this peptide is present within the slice preparation and the observed effects are not a result of constitutive activation of the CRHR1. Specifically, α-helical $CRH_{(9-41)}$ is a competitive antagonist that exhibits some partial agonist effects (Rainie et al. 1992), while NBI 30775 is an inverse agonist at the CRHR1 (Hoare et al. 2008). Thus, if CRHR1 was constitutively (or tonically) active we would likely observe divergent effects of the 2 antagonists with NBI 30775 reducing activation due to its inverse agonist properties, while α-helical $CRH_{(9-41)}$ would have no effect, or if anything (given its partial agonist properties) potentiate CRHR1 activity.

Implications for Hippocampal Function During Stress

We find that endogenously released CRH increases excitability of the hippocampus at single neuron and network levels, raising the possibility that state-dependent fluctuations in the concentration of the neuropeptide dynamically influence the structure's contributions to memory. Hippocampal CRH is rapidly released (within minutes) by stress (Chen et al. 2004b) and exposure to this peptide (stress-induced and exogenously applied) exerts dose and time-dependent effects upon hippocampal function. In general, acute stress or the brief application of exogenous CRH increases performance in a number of hippocampus-dependent behavioral tasks (Hung et al. 1992; Ma et al. 1999; Radulovic et al. 1999; Blank et al. 2002; Row and Dohanich 2008) while prolonged exposure impairs memory function in such tasks (Kim and Diamond 2002; McEwen 2006; Chen et al. 2010; Maras and Baram 2012). A significant body of work found evidence that hippocampal SPWs are critical to the consolidation of newly acquired memories and to the replay of already established ones (Atherton et al. 2015; Buzsaki 2015; Colgin 2016). Thus, our results showing that endogenous CRH modulates the frequency of SPWs delineate a novel mechanism for the potent influence of stress on memory. Indeed, consistent with such a proposed role, CRH has been implicated in memory consolidation and retention in a number of studies (Hung et al. 1992; Lee et al. 1996; Wu et al. 1997). Elucidating the temporal profile of the effects of CRH upon synaptic function and SPWs during stress, and the manner in which this peptide interacts with other stress-released mediators (e.g., glucocorticoids and noradrenaline), will be essential for evaluating the full extent of the contributions of hippocampal CRH to stress-induced alterations of memory (Joels and Baram 2009).

Supplementary Material

Supplementary material is available at *Cerebral Cortex* online.

Funding

National Institutes of Health (grant numbers NS28912, MIH73136, NS045260, NS085709) and from Deutsche Forschungsgemeinshaft (FR 620/ 14-1) for supporting this study.

Notes

The authors would like to dedicate this study to the memory of Dr Wylie Vale. *Conflict of Interest*: None declared.

References

Aldenhoff JB, Gruol DL, Rivier J, Vale W, Siggins GR. 1983. Corticotropin releasing factor decreases postburst hyperpolarizations and excites hippocampal neurons. Science. 221: 875–877.

Amaral DG, Witter MP. 1989. The three-dimensional organization of the hippocampal formation: a review of anatomical data. Neuroscience. 31:571–591.

Atherton LA, Dupret D, Mellor JR. 2015. Memory trace replay: the shaping of memory consolidation by neuromodulation. Trends Neurosci. 38:560–570.

Bajo M, Cruz MT, Siggins GR, Messing R, Roberto M. 2008. Protein kinase C epsilon mediation of CRF- and ethanol-induced GABA release in central amygdala. Proc Natl Acad Sci USA. 105:8410–8415.

Blank T, Nijholt I, Eckart K, Spiess J. 2002. Priming of long-term potentiation in mouse hippocampus by corticotropin-releasing factor and acute stress: implications for hippocampus-dependent learning. J Neurosci. 22:3788–3794.

Buzsaki G. 1986. Hippocampal sharp waves: their origin and significance. Brain Res. 398:242–252.

Buzsaki G. 1989. Two-stage model of memory trace formation: a role for "noisy" brain states. Neuroscience. 31:551–570.

Buzsaki G. 2015. Hippocampal sharp wave-ripple: a cognitive biomarker for episodic memory and planning. Hippocampus. 25:1073–1188.

Caliskan G, Schulz SB, Gruber D, Behr J, Heinemann U, Gerevich Z. 2015. Corticosterone and corticotropin-releasing factor acutely facilitate gamma oscillations in the hippocampus in vitro. Eur J Neurosci. 41:31–44.

Chattarji S, Tomar A, Suvrathan A, Ghosh S, Rahman MM. 2015. Neighborhood matters: divergent patterns of stress-induced plasticity across the brain. Nat Neurosci. 18:1364–1375.

Chen Y, Andres AL, Frotscher M, Baram TZ. 2012. Tuning synaptic transmission in the hippocampus by stress: the CRH system. Front Cell Neurosci. 6:13.

Chen Y, Bender RA, Frotscher M, Baram TZ. 2001. Novel and transient populations of corticotropin-releasing hormone-expressing neurons in developing hippocampus suggest unique functional roles: a quantitative spatiotemporal analysis. J Neurosci. 21:7171–7181.

Chen Y, Bender RA, Brunson KL, Pomper JK, Grigoriadis DE, Wurst W, Baram TZ. 2004a. Modulation of dendritic differentiation by corticotropin-releasing factor in the developing hippocampus. Proc Natl Acad Sci USA. 101:15782–15787.

Chen Y, Brunson KL, Adelmann G, Bender RA, Frotscher M, Baram TZ. 2004b. Hippocampal corticotropin releasing hormone: pre- and postsynaptic location and release by stress. Neuroscience. 126:533–540.

Chen Y, Brunson KL, Muller MB, Cariaga W, Baram TZ. 2000. Immunocytochemical distribution of corticotropin-releasing hormone receptor type-1 (CRF_1)-like immunoreactivity in the

mouse brain: light microscopy analysis using an antibody directed against the C-terminus. J Comp Neurol. 420:305–323.

Chen Y, Dube CM, Rice CJ, Baram TZ. 2008. Rapid loss of dendritic spines after stress involves derangement of spine dynamics by corticotropin-releasing hormone. J Neurosci. 28:2903–2911.

Chen C, Grigoriadis DE. 2005. NBI 30775 (R121919), an orally active antagonist of the corticotropin-releasing factor (CRF) type 1 receptor for the treatment of anxiety and depression. Drug Dev Res. 65:216–226.

Chen Y, Molet J, Gunn BG, Ressler K, Baram TZ. 2015. Diversity of reporter expression patterns in transgenic mouse lines targeting corticotropin-releasing hormone-expressing neurons. Endocrinology. 156:4769–4780.

Chen Y, Rex CS, Rice CJ, Dube CM, Gall CM, Lynch G, Baram TZ. 2010. Correlated memory defects and hippocampal dendritic spine loss after acute stress involve corticotropin-releasing hormone signaling. Proc Natl Acad Sci USA. 107:13123–13128.

Colgin LL. 2016. Rhythms of the hippocampal network. Nat Rev Neurosci. 17:239–249.

Farrant M, Nusser Z. 2005. Variations on an inhibitory theme: phasic and tonic activation of $GABA_A$ receptors. Nat Rev Neurosci. 6:215–229.

Hajos N, Karlocai MR, Nemeth B, Ulbert I, Monyer H, Szabo G, Erdelyi F, Freund TF, Gulyas AI. 2013. Input-output features of anatomically identified CA3 neurons during hippocampal sharp wave/ripple oscillation in vitro. J Neurosci. 33: 11677–11691.

Haug T, Storm JF. 2000. Protein kinase A mediates the modulation of the slow Ca^{2+}-dependent K^+ current, I_{sAHP}, by the neuropeptides CRF, VIP, and CGRP in hippocampal pyramidal neurons. J Neurophysiol. 83:2071–2079.

Herman MA, Kallupi M, Luu G, Oleata CS, Heilig M, Koob GF, Ciccocioppo R, Roberto M. 2013. Enhanced GABAergic transmission in the central nucleus of the amygdala of genetically selected Marchigian Sardinian rats: alcohol and CRF effects. Neuropharmacology. 67:337–348.

Hoare SR, Fleck BA, Gross RS, Crowe PD, Williams JP, Grigoriadis DE. 2008. Allosteric ligands for the corticotropin releasing factor type 1 receptor modulate conformational states involved in receptor activation. Mol Pharmacol. 73:1371–1380.

Hollrigel GS, Chen K, Baram TZ, Soltesz I. 1998. The proconvulsant actions of corticotropin-releasing hormone in the hippocampus of infant rats. Neuroscience. 84:71–79.

Hung HC, Chou CK, Chiu TH, Lee EH. 1992. CRF increases protein phosphorylation and enhances retention performance in rats. Neuroreport. 3:181–184.

Joels M, Baram TZ. 2009. The neuro-symphony of stress. Nat Rev Neurosci. 10:459–466.

Kaeser PS, Regehr WG. 2014. Molecular mechanisms for synchronous, asynchronous, and spontaneous neurotransmitter release. Annu Rev Physiol. 76:333–363.

Keegan CE, Karolyi IJ, Knapp LT, Bourbonais FJ, Camper SA, Seasholtz AF. 1994. Expression of corticotropin-releasing hormone transgenes in neurons of adult and developing mice. Mol Cell Neurosci. 5:505–514.

Kim JJ, Diamond DM. 2002. The stressed hippocampus, synaptic plasticity and lost memories. Nat Rev Neurosci. 3:453–462.

Klausberger T, Somogyi P. 2008. Neuronal diversity and temporal dynamics: the unity of hippocampal circuit operations. Science. 321:53–57.

Koniaris E, Drimala P, Sotiriou E, Papatheodoropoulos C. 2011. Different effects of zolpidem and diazepam on hippocampal sharp wave-ripple activity in vitro. Neuroscience. 175: 224–234.

Kratzer S, Mattusch C, Metzger MW, Dedic N, Noll-Hussong M, Kafitz KW, Eder M, Deussing JM, Holsboer F, Kochs E, et al. 2013. Activation of CRH receptor type 1 expressed on glutamatergic neurons increases excitability of CA1 pyramidal neurons by the modulation of voltage-gated ion channels. Front Cell Neurosci. 7:91.

Kubota D, Colgin LL, Casale M, Brucher FA, Lynch G. 2003. Endogenous waves in hippocampal slices. J Neurophysiol. 89:81–89.

Lee EH, Huang AM, Tsuei KS, Lee WY. 1996. Enhanced hippocampal corticotropin-releasing factor gene expression associated with memory consolidation and memory storage in rats. Chin J Physiol. 39:197–203.

Lupien SJ, McEwen BS, Gunnar MR, Heim C. 2009. Effects of stress throughout the lifespan on the brain, behaviour and cognition. Nat Rev Neurosci. 10:434–445.

Ma YL, Chen KY, Wei CL, Lee EH. 1999. Corticotropin-releasing factor enhances brain-derived neurotrophic factor gene expression to facilitate memory retention in rats. Chin J Physiol. 42:73–81.

Maier N, Nimmrich V, Draguhn A. 2003. Cellular and network mechanisms underlying spontaneous sharp wave-ripple complexes in mouse hippocampal slices. J Physiol. 550:873–887.

Maras PM, Baram TZ. 2012. Sculpting the hippocampus from within: stress, spines, and CRH. Trends Neurosci. 35: 315–324.

McEwen BS. 2006. Protective and damaging effects of stress mediators: central role of the brain. Dialogues Clin Neurosci. 8:367–381.

Migliore M, Morse TM, Davison AP, Marenco L, Shepherd GM, Hines ML. 2003. ModelDB: making models publicly accessible to support computational neuroscience. Neuroinformatics. 1(1): 135–139.

Neher E. 1992. Correction for liquid junction potentials in patch clamp experiments. Methods Enzymol. 207:123–131.

Papatheodoropoulos C. 2008. A possible role of ectopic action potentials in the in vitro hippocampal sharp wave-ripple complexes. Neuroscience. 157:495–501.

Papatheodoropoulos C, Koniaris E. 2011. α_5GABA_A receptors regulate hippocampal sharp wave-ripple activity in vitro. Neuropharmacology. 60:662–673.

Pinsky PF, Rinzel J. 1994. Intrinsic and network rhythmogenesis in a reduced Traub model for CA3 neurons. J Comput Neurosci. 1:39–60.

Prescott SA, Sejnowski TJ, De Koninck Y. 2006. Reduction of anion reversal potential subverts the inhibitory control of firing rate in spinal lamina I neurons: towards a biophysical basis for neuropapthic pain. Mol Pain. 2:32.

Radulovic J, Ruhmann A, Liepold T, Spiess J. 1999. Modulation of learning and anxiety by corticotropin-releasing factor CRF and stress: differential roles of CRF receptors 1 and 2. J Neurosci. 19:5016–5025.

Rainie DG, Fernhout BJ, Shinnick-Gallagher P. 1992. Differential actions of corticotropin releasing factor on basolateral and central amygdaloid neurones, in vitro. J Pharmacol Exp Ther. 263:846–858.

Ratte S, Hong S, De Schutter E, Prescott SA. 2013. Impact of neuronal properties on network coding: roles of spike initiation dynamics and robust synchrony transfer. Neuron. 78:758–772.

Refojo D, Schweizer M, Kuehne C, Ehrenberg S, Thoeringer C, Vogl AM, Dedic N, Schumacher M, von Wolff G, Avrabos C,

et al. 2011. Glutamatergic and dopaminergic neurons mediate anxiogenic and anxiolytic effects of CRHR1. Science. 333: 1903–1907.

Rex CS, Colgin LL, Jia Y, Casale M, Yanagihara TK, Debenedetti M, Gall CM, Kramar EA, Lynch G. 2009. Origins of an intrinsic hippocampal EEG pattern. PLoS One. 4:e7761.

Ritchie AK, Kuryshev YA, Childs GV. 1996. Corticotropin-releasing hormone and calcium signaling in corticotropes. Trends Endocrinol Metab. 7:365–369.

Row BW, Dohanich GP. 2008. Post-training administration of corticotropin-releasing hormone (CRH) enhances retention of a spatial memory through a noradrenergic mechanism in male rats. Neurobiol Learn Mem. 89:370–378.

Rudolph S, Tsai MC, von Gersdorff H, Wadiche JI. 2015. The ubiquitous nature of multivesicular release. Trends Neurosci. 38: 428–438.

Sakanaka M, Shibasaki T, Lederis K. 1986. Distribution and efferent projections of corticotropin-releasing factor-like immunoreactivity in the rat amygdaloid complex. Brain Res. 382:213–238.

Scanziani M, Capogna M, Gahwiler BH, Thompson SM. 1992. Presynaptic inhibition of miniature excitatory synaptic currents by baclofen and adenosine in the hippocampus. Neuron. 9:919–927.

Schlingloff D, Kali S, Freund TF, Hajos N, Gulyas AI. 2014. Mechanisms of sharp wave initiation and ripple generation. J Neurosci. 34:11385–11398.

Schneggenburger R, Rosenmund C. 2015. Molecular mechanisms governing Ca^{2+} regulation of evoked and spontaneous release. Nat Neurosci. 18:935–941.

Smith BN, Dudek FE. 1994. Age-related epileptogenic effects of corticotropin-releasing hormone in the isolated CA1 region of rat hippocampal slices. J Neurophysiol. 72:2328–2333.

Stimberg M, Goodman DF, Benichoux V, Brette R. 2014. Equation-oriented specification of neural models for simulations. Front Neuroinform. 8:6.

Swanson LW, Wyss JM, Cowan WM. 1978. An autoradiographic study of the organization of intrahippocampal association pathways in the rat. J Comp Neurol. 181:681–715.

Takuma K, Matsuda T, Yoshikawa T, Kitanaka J, Gotoh M, Hayata K, Baba A. 1994. Corticotropin-releasing factor stimulates Ca^{2+} influx in cultured rat astrocytes. Biochem Biophys Res Commun. 199:1103–1107.

Taxidis J, Coombes S, Mason R, Owen MR. 2012. Modeling sharp wave-ripple complexes through a CA3-CA1 network model with chemical synapses. Hippocampus. 22:995–1017.

Urban NN, Barrionuevo G. 1998. Active summation of excitatory postsynaptic potentials in hippocampal CA3 pyramidal neurons. Proc Natl Acad Sci USA. 95:11450–11455.

van den Pol AN. 2012. Neuropeptide transmission in brain circuits. Neuron. 76:98–115.

Wang XJ, Buzsaki G. 1996. Gamma oscillation by synaptic inhibition in a hippocampal interneuronal network model. J Neurosci. 16:6402–6413.

Wu C, Asl MN, Gillis J, Skinner FK, Zhang L. 2005. An in vitro model of hippocampal sharp waves: regional initiation and intracellular correlates. J Neurophysiol. 94:741–753.

Wu HC, Chen KY, Lee WY, Lee EH. 1997. Antisense oligonucleotides to corticotropin-releasing factor impair memory retention and increase exploration in rats. Neuroscience. 78: 147–153.

Yan XX, Toth Z, Schultz L, Ribak CE, Baram TZ. 1998. Corticotropin-releasing hormone (CRH)-containing neurons in the immature rat hippocampal formation: light and electron microscopic features and colocalization with glutamate decarboxylase and parvalbumin. Hippocampus. 8:231–243.